Contributions of Trans-boundary Transport to Summertime Air Quality in Beijing, China

Jiarui Wu[1,3], Guohui Li[1*], Junji Cao[1*], Naifang Bei[2], Yichen Wang[1], Tian Feng[1,2], Rujin Huang[1], Suixin Liu[1], Qiang Zhang[4], and Xuexi Tie[1]

[1]Key Lab of Aerosol Chemistry and Physics, SKLLQG, Institute of Earth Environment, Chinese Academy of Sciences, Xi'an, China
[2]School of Human Settlements and Civil Engineering, Xi'an Jiaotong University, Xi'an, Shaanxi, China
[3]University of Chinese Academy of Science, Beijing, China
[4]Department of Environmental Sciences and Engineering, Tsinghua University, Beijing, China
[*]Correspondence to: Guohui Li (ligh@ieecas.cn) and Junji Cao (jjcao@ieecas.cn)

Abstract: In the present study, the WRF-CHEM model is used to evaluate the contributions of trans-boundary transport to the air quality in Beijing during a persistent air pollution episode from 5 to 14 July 2015 in Beijing-Tianjin-Hebei (BTH), China. Generally, the predicted temporal variations and spatial distributions of $PM_{2.5}$ (fine particulate matter), O_3 (ozone), and NO_2 are in good agreement with observations in BTH. The WRF-CHEM model also reproduces reasonably well the temporal variations of aerosol species compared to measurements in Beijing. The factor separation approach is employed to evaluate the contributions of trans-boundary transport of non-Beijing emissions to the $PM_{2.5}$ and O_3 levels in Beijing. On average, in the afternoon during the simulation episode, the only-Beijing emissions contribute 22.4% to the O_3 level in Beijing, less than 36.6% from non-Beijing emissions. The O_3 concentrations in Beijing are decreased by 5.1% in the afternoon due to interactions between local and outside emissions. The non-Beijing emissions play a dominant role in the $PM_{2.5}$ level in Beijing, with a contribution of 61.5%, much higher than 13.7% from Beijing local emissions. The emissions interactions between local and outside emissions enhance the $PM_{2.5}$ concentrations in Beijing, with a contribution of 5.9%. Therefore, the air quality in Beijing is generally determined by the trans-boundary transport of non-Beijing emissions during summertime, showing that the cooperation with neighboring provinces to mitigate pollutant emissions is a key for Beijing to improve air quality.

32

33 ## 1 Introduction

34 Beijing, the capital of China, has become an environmentally stressed city due to
35 growing population, increasing transportation activity, and city expansion (Parrish and Zhu,
36 2009). Beijing is situated in northeastern China, surrounded from the southwest to the
37 northeast by the Taihang Mountains and the Yanshan Mountains and open to the North China
38 Plain (NCP) in the south and east. Unfortunately, NCP has become one of the most polluted
39 areas in China due to rapid industrialization and urbanization (Zhang et al., 2013). When
40 south or east winds are prevalent in NCP, air pollutants originated from NCP are transported
41 to Beijing and surrounding areas and subject to be accumulated due to the mountain blocking,
42 causing heavy air pollution in Beijing (Long et al., 2016).

43 $PM_{2.5}$ (fine particulate matter) and O_3 (ozone) are considered to be the most serious air
44 pollutants of concern in Beijing during summertime (e.g., Xie et al., 2015; Zheng et al., 2015;
45 Chen et al., 2015; Wang et al., 2016). The mean summertime $PM_{2.5}$ mass concentration is
46 about 80 μg m^{-3} in 2013 (Li et al., 2015a), exceeding the second grade of National Ambient
47 Air Quality Standards (NAAQS) in China and also higher than the average $PM_{2.5}$
48 concentration of 78.1 μg m^{-3} during the period from 2004 to 2012 (Liu et al., 2015). During
49 haze pollution events in summer 2014, the $PM_{2.5}$ concentration generally reaches 100 μg m^{-3},
50 and even exceeds 150 μg m^{-3} in Beijing (Wang et al., 2016). An increasing O_3 trend has been
51 observed in Beijing from 2002 to 2010 (Wang et al., 2012; Wang et al., 2013). The average
52 maximum 1-h O_3 concentration has been reported to achieve 140 μg m^{-3} during summertime
53 of 2013 in Beijing (Wang et al., 2014a). Wang et al. (2016) have demonstrated that the
54 summertime O_3 mass concentration holds a high level in 2014 in Beijing, with a daily

55 average of up to 110 μg m^{-3}. Chen et al. (2015) have further shown that the average
56 maximum daily O_3 concentrations are higher than 150 μg m^{-3} during the summer in 2015 at
57 most of monitoring sites in Beijing.

58 In recent years, Beijing has implemented aggressive emission control strategies to
59 ameliorate the air quality (Parrish and Zhu, 2009). Both NO_x ($NO+NO_2$) and total VOCs
60 (volatile organic compounds) in Beijing have decreased linearly since 2002, while the
61 daytime average O_3 concentration still increases rapidly (Tang et al., 2009; Wang et al., 2012;
62 Zhang et al., 2014). Zhang et al. (2014) have highlighted the importance of the
63 trans-boundary transport and the cooperation with neighboring provinces to control the O_3
64 level in Beijing. Pollutants transported from outside of Beijing and formed locally together
65 determine the air quality in Beijing (Meng et al., 2006; Zhang et al., 2012).

66 Several studies have been performed to investigate the role of trans-boundary transport
67 in the air quality of Beijing based on observational analyses and model simulations. Using the
68 US EPA's Model-3/CMAQ model simulation in the Beijing area, Streets et al. (2007) have
69 pointed out that Hebei Province can contribute 50-70% of Beijing's $PM_{2.5}$ concentration and
70 20-30% of O_3 concentration. Wang et al. (2009) have indicated that O_3 formation in Beijing
71 is not only affected by local emissions, but also influenced by Tianjin and the south of Hebei
72 Province. The intense regional transport of pollutants from south to north in NCP has been
73 proposed to be the main reason for the heavy haze pollution in January 2013 in Beijing (Sun
74 et al., 2014; Tao et al., 2014; Wang et al., 2014b). Jiang et al. (2015) have demonstrated that
75 the transport from the environs of Beijing contributes about 55% of the peak $PM_{2.5}$
76 concentration in the city during a heavy haze event in December 2013.

77 Since September 2013, the 'Atmospheric Pollution Prevention and Control Action Plan'
78 (hereafter referred to as APPCAP) has been implemented, which is released by the Chinese
79 State Council to reduce $PM_{2.5}$ by up to 25% by 2017 relative to 2012 levels. After
80 implementation of the APPCAP, high $PM_{2.5}$ mass concentrations still can be observed and
81 the O_3 pollution has deteriorated during summertime since 2013 in Beijing (Chen et al., 2015;
82 Wang et al., 2016). Hence, studies are imperative to explore the O_3 and $PM_{2.5}$ formation from
83 various sources and evaluate the pollutants contributions from local production and
84 trans-boundary transport in Beijing, to support the design of mitigation strategies.

85 The purpose of the present study is to evaluate the contributions of trans-boundary
86 transport of emissions outside of Beijing to the air quality in Beijing and interaction of
87 emissions in and outside of Beijing after APPCAP using the WRF-CHEM model. The model
88 configuration and methodology are described in Section 2. Model results and sensitivity
89 studies are presented in Section 3, and conclusions and discussions are given in Section 4.

90

91 ## 2 Model and Methodology

92 ### 2.1 WRF-CHEM Model

93 The WRF-CHEM model used in the study is developed by Li et al. (2010, 2011a, b,
94 2012) at the Molina Center for Energy and the Environment, with a new flexible gas phase
95 chemical module and the CMAQ aerosol module developed by US EPA. The aerosol
96 component of the Community Multiscale Air Quality (CMAQ) model is designed to be an
97 efficient and economical depiction of aerosol dynamics in the atmosphere (Binkowski and
98 Roselle, 2003). The particle size distribution in the study is represented as the superposition

of three lognormal subdistributions, called modes, which includes the processes of coagulation, particle growth by the addition of mass, and new particle formation. Following the work of Kulmala et al. (1998), the new particle production rate presented here is calculated as a parameterized function of temperature, relative humidity, and the vapor-phase H_2SO_4 concentration due to binary nucleation of H_2SO_4 and H_2O vapor, and the new particles are assumed to be 2.0 nm diameter. A number of recent studies have shown that organic compounds can play an important role in nucleation process (Zhang et al., 2009, 2012, 2015). The contribution from organic acids likely explains the high levels of aerosol, especially in polluted urban area, where large amount of organic acids can be emitted directly and produced by photochemical oxidation of hydrocarbons (Fan et al., 2006), which needs to be considered in the further study. The wet deposition follows the method used in the CMAQ and the surface deposition of chemical species is parameterized following Wesely (1989). The photolysis rates are calculated using the FTUV (Li et al., 2005; Li et al., 2011a), in which the effects of aerosols and clouds on photolysis are considered.

The inorganic aerosols are predicted in the WRF-CHEM model using ISORROPIA Version 1.7 (Nenes et al., 1998). The efficient and rapid secondary species formation in Beijing has been found during the severe haze formation process in the previous study (Guo et al., 2014). The secondary organic aerosol (SOA) formation is calculated using a non-traditional SOA module. The volatility basis-set (VBS) modeling method is used in the module, assuming that primary organic components are semi-volatile and photochemically reactive and are distributed in logarithmically spaced volatility bins. Detailed information about the volatility basis-set approach can be found in Li et al (2011b). Recent studies have

shown that small di-carbonyls (glyoxal and methylglyoxal) are important for the aerosol formation due to their traffic origin (Zhao et al., 2006; Gomez et al., 2015). Li et al. (2011a) have indicated that glyoxal and methylglyoxal can contribute about 10% of the SOA in the urban area of Mexico City. The SOA formation from glyoxal and methylglyoxal in this study is parameterized as a first-order irreversible uptake by aerosol particles and cloud droplets, with a reactive uptake coefficient of 3.7×10^{-3} for glyoxal and methylglyoxal (Zhao et al., 2006; Volkamer et al., 2007; Gomez et al., 2015).

2.2 Model Configuration

A persistent air pollution episode from 5 to 14 July 2015 in Beijing-Tianjin-Hebei (BTH) is simulated using the WRF-CHEM model. During the episode, the observed mean daily $PM_{2.5}$ concentration is 73.8 μg m^{-3} and the average O_3 concentration in the afternoon reaches 237.0 μg m^{-3} in Beijing. The maximum of O_3 concentration is higher than 350 μg m^{-3}, and the maximum of $PM_{2.5}$ concentration can reach a high level exceeding 150 μg m^{-3}. In supplement information (SI) section, SI-Figures 1a-c show the daily averages of the temperature, relative humidity, and wind speed in Beijing during the summer of 2015. The minimum air temperature is 18.7 °C, and the maximum air temperature is 40 °C during the summer, with average of 25.7 °C. The average relative humidity is 63.8%. The southeast or southwest wind is prevailing over NCP due to the influence of East Asian summer monsoon (Zhang et al., 2010), with the average wind speed of 5.6 m s^{-1} in the summer of 2015. During the study period, the average temperature, relative humidity, and wind speed are 28.4 °C, 51.7% and 6.3 m s^{-1}, respectively, indicating typical summertime meteorological conditions. During the summer of 2015, the average $PM_{2.5}$ concentration is 56.1 μg m^{-3} and the average O_3

concentration in the afternoon is 216.4 μg m^{-3} (SI-Figures 1d-e). The high O_3 and $PM_{2.5}$ event occurs frequently during the summertime of 2015, so the study period can well represent the summertime O_3 and $PM_{2.5}$ pollution in Beijing, and provides a suitable case for observation analyses and model simulations to investigate the effect of trans-boundary transport on the summertime air quality of Beijing.

The WRF-CHEM model adopts one grid with horizontal resolution of 6 km and 35 sigma levels in the vertical direction, and the grid cells used for the domain are 200 × 200 (Figure 1). The physical parameterizations include the microphysics scheme of Hong et al (Hong and Lim, 2006), the Mellor, Yamada, and Janjic (MYJ) turbulent kinetic energy (TKE) planetary boundary layer scheme (Janjić, 2002), the Unified Noah land-surface model (Chen and Dudhia, 2001), the rapid radiative transfer model (RRTM) long wave radiation scheme (Mlawer et al., 1997) and the Goddard shortwave parameterization (Suarex and Chou, 1994; Chou and Suarez, 1999). The NCEP 1° × 1° reanalysis data are used to obtain the meteorological initial and boundary conditions, and the meteorological simulations are not nudged in the study. The chemical initial and boundary conditions are interpolated from the 6h output of MOZART (Horowitz et al., 2003). The spin-up time of the WRF-CHEM model is 28 hours. The SAPRC-99 (Statewide Air Pollution Research Center, version 1999) chemical mechanism is used in the present study.

The anthropogenic emissions are developed by Zhang et al. (2009), which is based on the 2013 emission inventory, including contributions from agriculture, industry, power generation, residential, and transportation sources. The SO_2, NO_x, and CO emissions have been adjusted according to their observed trends from 2013 to 2015 in the present study, but

the VOCs emissions are not changed considering that the VOCs emissions are still not fully considered in the current air pollutant control strategy. The major pollutants emissions used in the model simulation for Beijing, Tianjin, and the neighboring provinces (Hebei, Shanxi, and Shandong) are summarized in Table 1. Obviously, high anthropogenic emissions are distributed outside of Beijing, especially in Hebei and Shandong provinces. Figure 2 presents distributions of the emission rates of VOCs, NO_x, OC, and SO_2 in the simulation domain, showing that the anthropogenic emissions are generally concentrated in urban areas. It is worth noting that uncertainties of the emission inventory used in the study are still rather large taking into consideration the rapid changes in anthropogenic emissions that are not fully reflected in the current emission inventories, particularly since implementation of the APPCAP, and the complexity of pollutants precursors. For example, different VOCs types exhibit distinct kinetic behaviors, and as an important fraction of total VOCs in the urban atmosphere, aromatics are responsible for the photochemical O_3 production and secondary organic aerosol formation (Suh et al., 2003; Fan et al., 2004). In the SAPRC99, aromatics are lumped into ARO1 and ARO2. ARO1 mainly includes toluene, benzene, ethylbenzene, and other aromatics with reaction rate with OH (kOH) less than 2×10^4 ppm^{-1} min^{-1}. ARO2 includes xylene, trimethylbenzene, and other aromatics with kOH greater than 2×10^4 ppm^{-1} min^{-1}. Additionally, biogenic VOCs also play a considerable role in the O_3 production (Li et al., 2007), and monoterpenes and isoprene are the main biogenic VOCs in the SAPRC99 chemical mechanism. The biogenic emissions are calculated online using the MEGAN (Model of Emissions of Gases and Aerosol from Nature) model developed by Guenther et al (2006).

2.3 Factor Separation Approach

The formation of the secondary atmospheric pollutant, such as O_3, secondary organic aerosol, and nitrate, is a complicated nonlinear process in which its precursors from various emission sources and transport react chemically or reach equilibrium thermodynamically. Nevertheless, it is not straightforward to evaluate the contributions from different factors in a nonlinear process. The factor separation approach (FSA) proposed by Stein and Alpert (1993) can be used to isolate the effect of one single factor from a nonlinear process and has been widely used to evaluate source effects (Gabusi et al., 2008; Weinroth et al., 2008; Carnevale et al., 2010; Li et al., 2014). The total effect of one factor in the presence of others can be decomposed into contributions from the factor and that from the interactions of all those factors.

Suppose that field $\boldsymbol{f}$ depends on a factor $\boldsymbol{\varphi}$:

$$\boldsymbol{f} = \boldsymbol{f}(\boldsymbol{\varphi})$$

The FSA decomposes function $\boldsymbol{f}(\boldsymbol{\varphi})$ into a constant part that does not depend on $\boldsymbol{\varphi}$ $(\boldsymbol{f}(\mathbf{0}))$ and a $\boldsymbol{\varphi}$-depending component $(\boldsymbol{f}'(\boldsymbol{\varphi}))$, as follows:

$$\boldsymbol{f}'(\mathbf{0}) = \boldsymbol{f}(\mathbf{0})$$

$$\boldsymbol{f}'(\boldsymbol{\varphi}) = \boldsymbol{f}(\boldsymbol{\varphi}) - \boldsymbol{f}(\mathbf{0})$$

Considering that there are two factors X and Y that influence the formation of secondary pollutants in the atmosphere and also interact with each other. Denoting $\boldsymbol{f_{XY}}$, $\boldsymbol{f_X}$, $\boldsymbol{f_Y}$, and $\boldsymbol{f_0}$ as the simulations including both of two factors, factor X only, factor Y only, and none of the two factors, respectively. The pure contributions of factor X and Y can be isolated as follows:

$$f'_X = f_X - f_0$$

$$f'_Y = f_Y - f_0$$

Note that term $f'_{X(Y)}$ represents the pure impacts of factor *X(Y)*, while f_0 is the term independent of factors *X* and *Y*.

The simulation including both factors *X* and *Y* is given by:

$$f_{XY} = f_0 + f'_X + f'_Y + f'_{XY}$$

The mutual interaction between *X* and *Y* can be expressed as:

$$f'_{XY} = f_{XY} - f_0 - f'_X - f'_Y = f_{XY} - (f_X - f_0) - (f_Y - f_0) - f_0 = f_{XY} - f_X - f_Y + f_0$$

The above equation shows that the study needs four simulations, f_{XY}, f_X, f_Y and f_0, to evaluate the contributions of two factors and their synergistic interactions.

2.4 Statistical Methods for Comparisons

In the present study, the mean bias (*MB*), root mean square error (*RMSE*) and the index of agreement (*IOA*) are used as indicators to evaluate the performance of WRF-CEHM model in simulation against measurements. *IOA* describes the relative difference between the model and observation, ranging from 0 to 1, with 1 indicating perfect agreement.

$$MB = \frac{1}{N}\sum_{i=1}^{N}(P_i - O_i)$$

$$RMSE = \left[\frac{1}{N}\sum_{i=1}^{N}(P_i - O_i)^2\right]^{\frac{1}{2}}$$

$$IOA = 1 - \frac{\sum_{i=1}^{N}(P_i - O_i)^2}{\sum_{i=1}^{N}(|P_i - \overline{O}| + |O_i - \overline{O}|)^2}$$

where P_i and O_i are the predicted and observed pollutant concentrations, respectively. *N* is the total number of the predictions used for comparisons, and $\overline{P}$ and $\overline{O}$ represents the average of the prediction and observation, respectively.

2.5 Pollutants Measurements

The hourly measurements of O_3, NO_2, and $PM_{2.5}$ used in the study are downloaded from the website http://www.aqistudy.cn/. The submicron sulfate, nitrate, ammonium, and organic aerosols are observed by the Aerodyne Aerosol Chemical Speciation Monitor (ACSM), which is deployed at the National Center for Nanoscience and Technology (NCNST), Chinese Academy of Sciences, Beijing (Figure 1). The mass spectra of organic aerosols are analyzed using the Positive Matrix Factorization (PMF) technique to separate into four components: hydrocarbon-like organic aerosol (HOA)，cooking organic aerosol (COA)，coal combustion organic aerosol (CCOA), and oxygenated organic aerosol (OOA). HOA, COA, and CCOA are interpreted as surrogates of primary organic aerosol (POA), and OOA is a surrogate of SOA.

The APPCAP has been implemented since 2013 September, so comparisons of summertime pollutants between 2013 and 2015 can show the mitigation effects on the air quality. Considering that high O_3 concentrations generally take place in the afternoon during summertime, Table 2 presents the summertime concentrations of pollutants in the afternoon (12:00 – 18:00 Beijing Time (BJT)) averaged at 12 monitoring sites in Beijing in 2013 and 2015. The rainy days during summertime in Beijing are 43 and 46 days in 2013 and 2015, respectively, showing the similar meteorological conditions between the two years. Therefore, in general, the air pollutants variations between 2013 and 2015 can be mainly attributed to implementation of the APPCAP. Apparently, implementation of the APPCAP has considerably decrease the concentrations of primary species of CO and SO_2, particularly with regard to SO_2, reduced by more than 40% from 2013 to 2015. Most of NO_x exist in the form of NO_2 in the afternoon during summertime due to active photochemical processes. Therefore,

25.1% decrease of NO_2 in the afternoon from 2013 to 2015 shows that the NO_x emission mitigation is also effective in Beijing. The $PM_{2.5}$ concentrations are decreased by about 24.0% from 2013 to 2015, approaching the expected 25% reduction by 2017 relative to 2012 levels. However, the O_3 trend is not anticipated in Beijing, and O_3 concentrations are increased from 133.0 μg m^{-3} in 2013 to 163.2 μg m^{-3} in 2015, enhanced by 22.8%. For the discussion convenience, we have defined the O_3 exceedance with hourly O_3 concentrations exceeding 200 μg m^{-3} and $PM_{2.5}$ exceedance with hourly $PM_{2.5}$ concentrations exceeding 75 μg m^{-3}. Although the $PM_{2.5}$ exceedance frequency in the afternoon has been decreased by 25.0% from 2013 to 2015, but still remains 32.7% in 2015. The O_3 exceedance frequency in 2015 is 31.8%, enhanced by 57.6% compared to 20.2% in 2013. Hence, during the summertime of 2015, two years after implementation of the APPCAP, Beijing still has experienced high O_3 and/or $PM_{2.5}$ pollutions frequently.

3 Results and Discussions

3.1 Model Performance

The hourly measurements of O_3, NO_2, and $PM_{2.5}$ in Beijing-Tianjin-Hebei (BTH) and ACSM measured aerosol species in Beijing are used to validate the WRF-CHEM model simulations.

3.1.1 O_3, NO_2, and $PM_{2.5}$ Simulations in Beijing

Figure 3 shows the temporal variations of observed and simulated near-surface O_3, NO_2, and $PM_{2.5}$ concentrations averaged over monitoring sites in Beijing from 5 to 14 July 2015. The WRF-CHEM model performs reasonably well in simulating the $PM_{2.5}$ variations

compared with observations in Beijing. The *MB* and *RMSE* are -3.6 μg m^{-3} and 22.5 μg m^{-3}, respectively, and the *IOA* is 0.86. The model well reproduces the temporal variations of O_3 concentrations, with an *IOA* of 0.92. The model considerably underestimates the O_3 concentration during daytime on July 5, 6 and 13. Most of monitoring sites in Beijing are concentrated in the urban area. Therefore, if the simulated winds cause the O_3 plume formed in the urban area to leave early or deviate the O_3 plume transported from outside of Beijing from the urban area, the model is subject to underestimate the O_3 concentration in Beijing (Bei et al., 2010). The WRF-CHEM model also reasonably yields the NO_2 diurnal profiles, but frequently overestimates the NO_2 concentrations during nighttime, which is likely caused by the biased boundary layer simulations.

3.1.2 Aerosol Species Simulations in Beijing

Figure 4 shows the temporal variations of simulated and observed aerosol species at NCNST site in Beijing from 5 to 14 July 2015. The WRF-CHEM model generally performs reasonably in simulating the aerosol species variations compared with ACSM measurements. As a primary aerosol species, the POA in Beijing is determined by direct emissions from various sources and transport from outside of Beijing, so uncertainties from emissions and meteorological fields remarkably affect the model simulations (Bei et al., 2012;Bei et al., 2013). Although the *MB* and *RMSE* for POA are 0.0 μg m^{-3} and 3.1 μg m^{-3}, respectively, the *IOA* is less than 0.60, indicating the considerable biases in POA simulations. The WRF-CHEM model has difficulties in well simulating the sulfate aerosol, with an *IOA* lower than 0.60. The model cannot produce the observed high peaks of sulfate aerosols around noontime on 8, 11, and 12 July 2015. The sulfate aerosol in the atmosphere is produced from

297 multiple sources, including SO_2 gas-phase oxidations by hydroxyl radicals (OH) and
298 stabilized criegee intermediates (sCI), aqueous reactions in cloud or fog droplets, and
299 heterogeneous reactions on aerosol surfaces, as well as direct emissions from power plants
300 and industries (Li et al., 2016). The model reasonably well reproduces the observed temporal
301 variations of SOA, nitrate, and ammonium, with *IOA*s exceeding 0.75. The model simulate
302 well the peak concentration of SOA, nitrate and ammonium at the rush hour, but the model
303 also underestimates the SOA, nitrate and ammonium as well, with *MB* of -1.1 μg m^{-3}, -0.7 μg
304 m^{-3}, and -0.5 μg m^{-3}, respectively. For nitrate and ammonium aerosols, the underestimation
305 occurs mainly on 8 July 2015.

306 **3.1.3 O_3, NO_2, and $PM_{2.5}$ Simulations in BTH**

307 Figure 5 shows the diurnal profiles of observed and simulated near-surface O_3, NO_2,
308 and $PM_{2.5}$ concentrations averaged over monitoring sites in BTH from 5 to 14 July 2015. The
309 WRF-CHEM model exhibits good performance in predicting the temporal variations of O_3,
310 NO_2, and $PM_{2.5}$ concentrations compared with measurements in BTH, with *IOA*s higher than
311 0.80. In addition, O_3 and NO_2 simulations are also improved in BTH compared to those in
312 Beijing, indicating better model performance for regional simulations in a large scale.

313 Figure 6 presents the distributions of calculated and observed near-surface $PM_{2.5}$
314 concentrations along with the simulated wind fields at 10:00 Beijing Time (BJT) on the six
315 selected representative days with high O_3 and $PM_{2.5}$ concentrations. The calculated $PM_{2.5}$
316 spatial patterns generally agree well with the observations at the monitoring sites. The
317 observed $PM_{2.5}$ concentrations in BTH are still high even after implementation of the
318 APPCAP, frequently exceeding 75 μg m^{-3} on the selected six days. The $PM_{2.5}$ concentrations

in Beijing are higher than 115 μg m^{-3} at 10:00 BJT on 8, 11, and 12 July 2015, causing moderate air pollution.

The O_3 concentration during summertime reaches its peak during the period from 14:00 to 16:00 BJT in Beijing (Tang et al., 2012). Figure 7 presents the spatial distribution of calculated and measured near-surface O_3 concentration at 15:00 Beijing Time (BJT) on the selected six days, along with the simulated wind fields. In general, the simulated O_3 spatial patterns are consistent with the measurements, but model biases still exist. High O_3 concentrations at 15:00 BJT in Beijing are observed and also simulated by the model, frequently exceeding 250 μg m^{-3}. The O_3 transport to Beijing from its surrounding areas is also obvious when the winds are easterly or southerly. Figure 8 provides the spatial distribution of simulated and observed near-surface NO_2 concentration on the selected six days at 08:00 BJT when the NO_2 concentration reaches it peak due to rush hour NO_x emissions and low planetary boundary layer (PBL). The simulated near-surface NO_2 concentrations highlights the dominant impact of the anthropogenic emissions, primarily concentrated in cities or their downwind areas, which generally agree well with the measurements. Beijing is surrounded from south to east by cities with high NO_2 concentrations, which can influence the O_3 formation in Beijing when south or east winds are prevalent.

The good agreements between predicted $PM_{2.5}$, O_3, NO_x and aerosol species and the corresponding measurements show that the modeled meteorological fields and emissions used in simulations are generally reasonable.

3.2 Contributions of Trans-boundary Transport to the O_3 and $PM_{2.5}$ Levels in Beijing

3.2.1 Analysis of Horizontal Transport of O_3 and $PM_{2.5}$

The analysis in Section 3.1.3 has shown the strong correlation between the airflow and the high level of pollutants in Beijing during the study episode. It is essential to confirm whether the continuous air pollutions in Beijing are directly related to the airflow transport from outside of Beijing (An et al., 2007; Yang et al., 2010). In the present study, the horizontal transport flux intensity is defined as the horizontal wind speed on the grid border multiplied by the pollutants concentration of the corresponding grid from which the airflows comes (Jiang et al., 2008). Considering that trans-boundary transport mainly occurs within the PBL, the study also focuses on the contribution of trans-boundary transport of pollutants within PBL over Beijing and its surrounding areas. Previous studies have shown that the average mixing layer height is approximately between 600 - 800 m during summertime, with the maximum during noontime higher than 1000 m (Wang et al., 2015;Tang et al., 2016). Figure 9 shows the temporal variations of net horizontal transport flux of $PM_{2.5}$, O_3 and NO_2 through Beijing boundary and the pollutants contributions from non-Beijing emissions to the air quality in Beijing city. The hourly $PM_{2.5}$, O_3 and NO_2 contributions of non-Beijing emissions generally have the same variation trend as the horizontal transport flux, indicating that the contribution of surrounding sources plays an important role in high pollutants concentrations in Beijing during the study episode. For example, the O_3 net flux also has the similar peak in the afternoon as the O_3 contribution from the non-Beijing emissions. As discussed in Section 3.1.3, the prevailing south wind dominates BTH, so the largest flux intensity are from the south, with the average of 103.3 g s^{-1} and 244.5 g s^{-1} for $PM_{2.5}$ and O_3, respectively (SI-Table 1), indicating that the pollutants are mainly from south. The average

horizontal transport fluxes for $PM_{2.5}$ and O_3 during the episode are 68.2 g s^{-1} and 68.5 g s^{-1}, respectively, showing important contributions of non-Beijing emissions to the air quality in Beijing.

3.2.2 Trans-boundary Transport Contributions to $PM_{2.5}$ and O_3 in Beijing

The FSA is used in the present study to evaluate the contributions and interactions of emissions from Beijing and outside of Beijing to the near-surface concentrations of O_3 and $PM_{2.5}$ in Beijing. Four model simulations are performed, including $\boldsymbol{f_{BS}}$ with both the anthropogenic emissions from Beijing and outside of Beijing, $\boldsymbol{f_B}$ with the emission from Beijing alone, $\boldsymbol{f_S}$ with only emissions outside of Beijing, and $\boldsymbol{f_0}$ without both the emissions from Beijing and outside of Beijing, representing background concentrations. Therefore, the air pollutants levels in Beijing are determined by the contribution from only-Beijing emissions ($\boldsymbol{f'_B}$, $\boldsymbol{f_B - f_0}$), the trans-boundary transport of non-Beijing emissions ($\boldsymbol{f'_S}$, $\boldsymbol{f_S - f_0}$), emission interactions between local and outside emissions ($\boldsymbol{f'_{BS}}$, $\boldsymbol{f_{BS} - f_B - f_S + f_0}$), and background ($\boldsymbol{f_0}$).

Figure 10 provides the temporal variations of the average near-surface O_3 and $PM_{2.5}$ concentrations from $\boldsymbol{f_{BS}}$ with all the emissions, $\boldsymbol{f_B}$ with Beijing emissions alone, and $\boldsymbol{f_S}$ with non-Beijing emissions alone in Beijing from 5 to 14 July 2015. Apparently, non-Beijing emissions generally play a more important role in the O_3 level of Beijing than only-Beijing emissions. Even when the Beijing local emissions are excluded, the O_3 concentration in Beijing still remains high level, with an average of 153 μg m^{-3} and ranging from 130 to 180 μg m^{-3} in the afternoon. When only considering the Beijing local emission in simulations, the afternoon average O_3 concentration in Beijing is approximately 126.6 μg m^{-3}, varying from

385 80 to 160 μg m^{-3}. On July 13, the contribution from Beijing local emissions exceeds that from
386 non-Beijing emissions because north winds are prevailing, bringing clean air to Beijing
387 (Figure 7f). Table 3 gives the average O_3 contributions from 12:00 to 18:00 BJT in Beijing
388 from only-Beijing emissions, non-Beijing emissions, emission interactions, and background.
389 The local emissions contribute about 22.4% on average in the afternoon to the O_3 level in
390 Beijing, varying from 15.5% to 35.4%. The outside emissions contribute more than local
391 sources, with an average contribution of 36.6%, ranging from 15.2% to 48.0%. The emission
392 interactions in Beijing decrease the O_3 level by 5.1% on average. O_3 formation is a nonlinear
393 process, depending on not only the absolute levels of NO_x and VOCs, but also the ratio of
394 VOC_s/NO_x (Sillman et al., 1990; Lei et al., 2007, 2008). When the O_3 precursors emitted
395 from outside of Beijing are transported to Beijing and mixed with local emissions, the
396 concentrations of O_3 precursors are increased and the ratio of VOC_s/NO_x is also altered,
397 causing the formed O_3 concentration unequal to the simple linear summation of O_3
398 contributions from the local and outside of Beijing emissions. The background O_3 in Beijing
399 plays an important role in the O_3 level in the afternoon, accounting for 46.1% of the O_3
400 concentration. The background O_3 contribution varies from 32.6% to 62.9% during the
401 episode, which is primarily determined by the prevailing wind direction. When the northerly
402 wind is prevalent, the clean airflow from the north affects Beijing, enhancing the background
403 O_3 contribution, such as on 5, 13, and 14 July 2015. However, when the polluted airflow
404 from the south impacts Beijing, the background O_3 contribution is decreased. The O_3
405 contributions in Beijing induced by the trans-boundary transport of emissions outside of
406 Beijing is about 31.5% of the O_3 concentration during the study episodes, indicating that the

407 trans-boundary transport constitutes the main reason for the elevated O_3 level in Beijing after
408 implementation of the APPCAP. Using the O_3 source apportionment technique, Wang et al.,
409 (2009) have emphasized that local emissions are the most important contributor to high O_3
410 levels from June to July in 2000 in Beijing urban area because the emissions rates there are
411 significantly higher than the average level in the surrounding areas. Based on CMAQ
412 simulations of Beijing, Streets et al., (2007) have estimated that 35%—60% of the high O_3
413 concentration at the Olympic Stadium site could be attributed to non-Beijing emissions, with
414 Hebei Province contributing 20%—30% of Beijing's O_3 concentration during the prevailing
415 south wind. Wang et al., (2008) have found that the average contribution from non-Beijing
416 emissions to the O_3 levels in Beijing is 30.0% and the maximum of daily contributions is as
417 high as 56.5% in August 2006.

418 Previous studies have proposed that the regional transport of O_3 precursors can play an
419 important role in inducing the high level in Beijing (Wang et al., 2009; Zhang et al.,2014).
420 SI-Table 2 provides the average NO_2 contributions in Beijing from only-Beijing emissions,
421 non-Beijing emissions, emission interactions, and background. Different from O_3, the local
422 emissions dominate the level of NO_2 in Beijing area, with an average contribution of 70.3%
423 during the study episode. The average contribution of non-Beijing emissions, emission
424 interactions and background are 24.8%, 0.9% and 4.0%, respectively. The contribution of
425 background to O_3 is obvious, which is much more different from that for NO_2. In addition,
426 the trans-boundary transport flux of NO_2 is much lower than O_3 (Figure 9). Given NO_x
427 lifetime in the summer is short, regional transport of NO_x is not important. Furthermore, the
428 emissions of NO_x and VOC_s around Beijing are much more than those in Beijing, especially

in Hebei and Shandong provinces, which is subject to contribute more O_3 production (Table 1). Compared to the direct input of regional O_3, the transport of O_3 precursors probably does not play an important role in the high O_3 level in Beijing.

When the Beijing local emissions are not considered in simulations, Beijing still experiences high $PM_{2.5}$ pollution, with an average $PM_{2.5}$ concentration of 48.3 μg m^{-3} during the simulation episode, and the $PM_{2.5}$ level in Beijing still exceeds 75 μg m^{-3} on several days. However, when only considering the Beijing local emissions, the average $PM_{2.5}$ concentration in Beijing is 19.6 μg m^{-3} during the episode, showing that Beijing's $PM_{2.5}$ pollution is dominated by the trans-boundary transport (Figure 10b). Table 4 shows the average $PM_{2.5}$ contribution in Beijing from only-Beijing emissions, non-Beijing emissions, emission interactions, and background. During the study episode, the average $PM_{2.5}$ contribution from local emissions is 13.7%, which is much lower than the contribution of 61.5% from the emissions outside of Beijing, further showing the dominant role of the trans-boundary transport in the Beijing $PM_{2.5}$ pollution. The emission interactions enhance the $PM_{2.5}$ level in Beijing on average, with a contribution of 5.9%. The background $PM_{2.5}$ contribution to Beijing is 18.9% on average, lower than those for O_3. The $PM_{2.5}$ contribution caused by the trans-boundary transport is about 67.4% of $PM_{2.5}$ concentrations in Beijing, indicating that the cooperation with neighboring provinces to control the $PM_{2.5}$ level is a key for Beijing to improve air quality. Previous studies have also demonstrated the dominant role of non-Beijing emission in the $PM_{2.5}$ level in Beijing. Based on CMAQ model, Streets et al., (2007) have reported that average contribution of regional transport to $PM_{2.5}$ at the Olympic Stadium can be 34%, up to 50%—70% under prevailing south winds. Guo et al. (2010) have

provided a rough estimation that the regional transport can contribute 69% of the PM_{10} and 87% of the $PM_{1.8}$ in Beijing local area using the short and low time resolution data in the summer. Combining the $PM_{2.5}$ observations and MM5-CMAQ model results, regional transport is estimated to contribute 54.6% of the $PM_{2.5}$ concentration during the polluted period, with an annual average $PM_{2.5}$ contribution of 42.4% (Lang et al., 2013). Using the long-term measurements of $PM_{2.5}$ mass concentrations from 2005 to 2010 at urban Beijing, and trajectory cluster and receptor models, the average contribution of long-distance transport to Beijing's $PM_{2.5}$ level can be approximately 75.2% in the summer (Wang et al., 2015).

Figure 11 shows the temporal variation of the averaged contributions to the near-surface aerosol constituents from total emissions ($\boldsymbol{f_{BS}}$), only-Beijing emissions ($\boldsymbol{f'_B}$), the trans-boundary transport of non-Beijing emissions ($\boldsymbol{f'_S}$), emission interactions ($\boldsymbol{f'_{BS}}$), and the background ($\boldsymbol{f_0}$) during the simulation episode. The temporal variations of elemental carbon (EC) and POA from local emissions and trans-boundary transport exhibit obvious diurnal cycles, e.g., highest during nighttime and lowest in the afternoon, corresponding to the variations of PBL height and anthropogenic emissions. The SOA from local emissions reaches its peak in the afternoon when the O_3 concentration is high, but the trans-boundary transport causes the gradual accumulation process of SOA in Beijing from July 5 to 9 and from July 9 to 13. The sulfate temporal profile from the trans-boundary transport is similar to that of SOA, also showing the accumulation process. In addition, the sulfate aerosols from only-Beijing emissions do not vary remarkably. The nitrate aerosols from only-local emissions and the trans-boundary transport generally attain peaks in the morning when the air temperature is not high and the HNO_3 concentrations are not low. The ammonium aerosol

473 variations are generally determined by those of sulfate and nitrate aerosols. For example, the
474 variations of ammonium aerosols from the trans-boundary include not only the morning
475 peaks, but also the accumulation processes from July 5 to 9 and from July 9 to 13. Except the
476 sulfate aerosol, the temporal variations of aerosol species from background are not large.

477 Table 5 presents the average aerosol constituents contributions from Beijing local
478 emissions, non-Beijing emissions, emission interactions, and the background, and mass
479 fractions in the total $PM_{2.5}$ in Beijing during the episode. Organic aerosols (POA+SOA)
480 constitute the most important component of $PM_{2.5}$, accounting for 34.8% of $PM_{2.5}$ mass
481 concentration, which is consistent with the ACSM measurement in Beijing (Sun et al., 2014).
482 In addition, SOA contributes more than 70% of organic aerosol mass concentrations, which is
483 due to the high atmospheric oxidation capability caused by elevated O_3 concentrations during
484 summertime. Although the SO_2 concentrations have been decreased by more than 40% since
485 implementation of the APPCAP, sulfate aerosols still play an important role in the $PM_{2.5}$
486 level in Beijing and make up 25.1% of the $PM_{2.5}$ mass concentrations, showing high sulfate
487 contributions from the trans-boundary transport and background. The ammonium, nitrate, EC,
488 and unspecified species account for 13.7%, 14.1%, 5.8%, and 6.5% of the $PM_{2.5}$ mass
489 concentrations, respectively. Secondary aerosol species dominate the $PM_{2.5}$ mass
490 concentration in Beijing, with a contribution of 77.9%, corresponding to the high atmospheric
491 oxidation capability.

492 The only-Beijing emissions contribute more than 20% of the mass concentrations for the
493 primary aerosol species, but less than 15% for the secondary aerosol species in Beijing (Table
494 5). The trans-boundary transport of non-Beijing emissions dominates all the aerosol species

levels in Beijing, with contributions exceeding 50%, particularly for SOA and nitrate. In addition, the POA and sulfate background contributions are also high, more than 20%. Although the primary aerosol species of EC and unspecified constituents are not involved in the chemical process and also do not participate in the gas-particle partitioning, the emission interactions still enhance EC and unspecified constituents concentrations, with contributions of around 1.5%, which is caused by the aerosol radiative effect. It is clear that the PBL-pollution interaction plays an important role in the pollutant accumulation in Beijing (Wang et al., 2013;Peng et al., 2016). Mixing of Beijing local emissions with those outside of Beijing increases the aerosol concentrations in the PBL and decreases the incoming solar radiation down to the surface, cooling the temperature of the low level atmosphere to suppress the development of PBL and hinder the aerosol dispersion in the vertical direction. The emission interactions increase the POA and SOA concentrations, with a POA contribution of 5.3% and a SOA contribution of 5.9%. In the VBS modeling approach, primary organic components are assumed to be semi-volatile and photochemically reactive. Mixing of Beijing local emissions with outside emissions enhances the organic condensable gases, and considering that the saturation concentrations of the organic condensable gases do not change, more organic condensable gases participate into the particle phase, increasing the POA and SOA concentrations. The contributions of emission interactions to inorganic aerosols, including sulfate, nitrate, and ammonium are more complicated, depending on their particle phase and precursors concentrations. In the present study, ISORROPIA (Version 1.7) is used to calculate the thermodynamic equilibrium between the sulfate-nitrate-ammonium-water aerosols and their gas phase precursors

517 H_2SO_4-HNO_3-NH_3-water vapor. Although mixing of Beijing local emissions with those
518 outside of Beijing increases inorganic aerosols precursors, the inorganic aerosol contributions
519 from emission interactions are still uncertain due to the deliberate thermodynamic
520 equilibrium between inorganic aerosols and their precursors. High atmospheric oxidation
521 capability induced by elevated O_3 concentration facilitates HNO_3 formation through NO_2
522 reaction with OH during daytime and N_2O_5 formation through NO_2 reaction with O_3 during
523 nighttime. High O_3 concentrations are produced by Beijing local emissions and those outside
524 of Beijing, accelerating the HNO_3 or N_2O_5 formation. Hence, mixing of Beijing local
525 emissions with those outside of Beijing considerably increases the HNO_3 or N_2O_5 levels,
526 pushing more HNO_3 or N_2O_5 into the particle phase. The nitrate contributions from emission
527 interactions are 18.1%, much more than those for other aerosol constituents. SO_2 gas-phase
528 oxidations by OH and sCI are not as fast as NO_2 reaction with OH, so the formation of
529 sulfuric acid is slow, although the O_3 concentration is high during summertime. Therefore,
530 the sulfate contributions from emission interactions is not significant, only 3.4%. As the
531 ammonium precursor, NH_3 is generally from direct emissions. The ammonium contributions
532 from emission interactions are 1.5%, similar to those of primary aerosol species that are
533 caused by aerosol radiative effects, indicating that the NH_3 emissions are not sufficiently high
534 in Beijing and outside of Beijing.
535
536 **4 Summary and Conclusions**
537 In the present study, a persistent air pollution episode with high concentrations of O_3
538 and $PM_{2.5}$ are simulated using the WRF-CHEM model during the period from July 5 to 14,

2015 in BTH, to evaluate the contributions of trans-boundary transport to the air quality in Beijing. Although the APPCAP has been implemented since 2013 September, the average O_3 concentration in the afternoon has been increased by 22.8% from 2013 to 2015 in Beijing, and Beijing still has experienced high O_3 and/or $PM_{2.5}$ pollutions frequently during summertime of 2015.

In general, the predicted temporal variations of $PM_{2.5}$, O_3, and NO_2 concentrations agree well with observations in Beijing and BTH, but the model biases still exist, which is perhaps caused by the uncertainties of simulated meteorological conditions and the emission inventory. The model also successfully reproduces the spatial distributions of $PM_{2.5}$, O_3, and NO_2 concentrations compared with measurements. The model performs reasonably well in modeling the variations of aerosol constituents compared with ACSM measurement at NCNST site in Beijing, but there are considerable biases in POA and sulfate simulations.

The FSA is used to investigate the contribution of trans-boundary transport of non-Beijing emissions to the air quality in Beijing. If the Beijing local emissions are not considered in model simulations, the O_3 and $PM_{2.5}$ concentrations in Beijing still remain high levels, showing that the trans-boundary transport of emissions outside of Beijing plays a more important role in the air quality in Beijing than the Beijing local emissions. On average, the only-Beijing emissions contribute 22.4% of O_3 in the afternoon and 13.7% of $PM_{2.5}$ mass concentrations in Beijing during the episode. The O_3 contribution in the afternoon and $PM_{2.5}$ contribution from the trans-boundary transport of non-Beijing emissions are 36.6% and 61.5%, respectively, far exceeding those from only-local emissions. The interactions between local and outside emissions generally decrease the O_3 level in the afternoon and increase the

561 $PM_{2.5}$ level in Beijing during the episode, with contributions of -5.1% and +4.4%,
562 respectively. In addition, the trans-boundary transport dominates all the aerosol species levels
563 in Beijing, with contributions exceeding 50% on average, particularly for SOA and nitrate.
564 The emission interactions in general increase all the aerosol species levels due to the aerosol
565 radiative effect and the enhancement of precursors of secondary aerosols. Hence, the air
566 quality in Beijing during summertime is generally determined by the trans-boundary transport
567 of emissions outside of Beijing. The cooperation with neighboring provinces to decrease
568 pollutant emissions is the optimum approach to mitigate the air pollution in Beijing. The FSA
569 method can calculate the individual and synergistic contribution of only-Beijing and
570 non-Beijing emissions by including or excluding the local or non-local emissions. However,
571 considering the nonlinear chemistry of $PM_{2.5}$ and O_3, especially regarding O_3 formation, the
572 method might not well provide how the air quality is accurately when taking different
573 emission reduction measures. Therefore, in the future study, sensitivity simulations of
574 different emission reduction measures are needed to design reasonable emission control
575 strategies.

576 It is worth noting that, although the WRF-CHEM model well captures the spatial
577 distributions and temporal variations of pollutants, the model biases still exist. The
578 discrepancies between the predictions and observations are possibly caused by the
579 uncertainties in the emission inventory and the meteorological fields simulations (Zhang et al.,
580 2015). Future studies need to be conducted to improve the WRF-CHEM model simulations,
581 and further to assess the contributions of trans-boundary transport of emissions outside of
582 Beijing to the air quality in Beijing, considering the rapid changes in anthropogenic

583 emissions since implementation of the APPCAP. In addition, simulations for more pollution
584 episodes should be investigated to evaluate the contribution of trans-boundary contributions
585 to the air quality in Beijing for supporting the design and implementation of emission control
586 strategies.
587
588 Data availability: The real-time O_3 and $PM_{2.5}$ are accessible for the public on the website
589 http://106.37.208.233:20035/. One can also access the historic profile of observed ambient
590 pollutants through visiting http://www.aqistudy.cn/.
591
592 *Acknowledgements.* This work was supported by the National Natural Science Foundation of
593 China (No. 41275153) and supported by the "Strategic Priority Research Program" of the
594 Chinese Academy of Sciences，Grant No. XDB05060500. Guohui Li is also supported by the
595 “Hundred Talents Program” of the Chinese Academy of Sciences. Naifang Bei is supported
596 by the National Natural Science Foundation of China (No. 41275101).
597

Reference

An, X., Zhu, T., Wang, Z., Li, C., and Wang, Y.: A modeling analysis of a heavy air pollution episode occurred in Beijing, Atmospheric Chemistry and Physics, 7, 3103-3114, 2007.

Bei, N., Lei, W., Zavala, M., and Molina, L. T.: Ozone predictabilities due to meteorological uncertainties in the Mexico City basin using ensemble forecasts, Atmospheric Chemistry and Physics, 10, 6295-6309, 10.5194/acp-10-6295-2010, 2010.

Bei, N., Li, G., and Molina, L. T.: Uncertainties in SOA simulations due to meteorological uncertainties in Mexico City during MILAGRO-2006 field campaign, Atmospheric Chemistry and Physics, 12, 11295-11308, 10.5194/acp-12-11295-2012, 2012.

Bei, N. F., Li, G. H., Zavala, M., Barrera, H., Torres, R., Grutter, M., Gutierrez, W., Garcia, M., Ruiz-Suarez, L. G., Ortinez, A., Guitierrez, Y., Alvarado, C., Flores, I., and Molina, L. T.: Meteorological overview and plume transport patterns during Cal-Mex 2010, Atmospheric Environment, 70, 477-489, 10.1016/j.atmosenv.2012.01.065, 2013.

Binkowski, F. S. and Roselle S. J.: Models-3 Community Multiscale Air Quality (CMAQ) model aerosol component: 1. Model description, J. Geophys. Res., 108, 4183, doi:10.1029/2001JD001409, 2003.

Carnevale, C., Pisoni, E., and Volta, M.: A non-linear analysis to detect the origin of PM10 concentrations in Northern Italy, Science of Total Environment, 409, 182-191, http://dx.doi.org/10.1016/j.scitotenv.2010.09.038, 2010.

Chen, F., and Dudhia, J.: Coupling an advanced land surface-hydrology model with the Penn State-NCAR MM5 modeling system. Part I: Model implementation and sensitivity, Mon. Weather Rev., 129, 569-585, 10.1175/1520-0493(2001)129<0569:caalsh>2.0.co;2, 2001.

Chen, W., Yan, L., and Zhao, H. M.: Seasonal Variations of Atmospheric Pollution and Air Quality in Beijing, Atmosphere, 6, 1753-1770, 10.3390/atmos6111753, 2015.

Chou, M. D., and Suarez, M. J.: A solar radiation parameterization for atmospheric studies, NASA TM-104606, Nasa Tech.memo, 15, 1999.

Chou, M. D., Suarez, M. J., Liang, X. Z., Yan, M. H., and Cote, C.: A Thermal Infrared Radiation Parameterization for Atmospheric Studies, Max J, 2001.

Fan, J. W., and Zhang, R. Y.: Atmospheric Oxidation Mechanism of Isoprene, Environmental Chemistry, 1, 140-149, 10.1071/en04045, 2004.

Fan, J. W., Zhang, R. Y., Collins, D., and Li, G. H.: Contribution of secondary condensable organics to new particle formation: A case study in Houston, Texas, Geophysical Research Letters, 33, 4, 10.1029/2006gl026295, 2006.

Gabusi, V., Pisoni, E., and Volta, M.: Factor separation in air quality simulations, Ecological Modelling, 218, 383-392, http://dx.doi.org/10.1016/j.ecolmodel.2008.07.030, 2008.

Gomez, M. E., Lin, Y., Guo, S., and Zhang, R. Y.: Heterogeneous Chemistry of Glyoxal on Acidic Solutions. An Oligomerization Pathway for Secondary Organic Aerosol Formation, Journal of Physical Chemistry A, 119, 4457-4463, 10.1021/jp509916r, 2015.

637 Guenther, A., Karl, T., Harley, P., Wiedinmyer, C., Palmer, P. I., and Geron, C.: Estimates of
638 global terrestrial isoprene emissions using MEGAN (Model of Emissions of Gases and
639 Aerosols from Nature), Atmospheric Chemistry and Physics, 6, 3181-3210, 2006.

640 Guo, S., Hu, M., Zamora, M. L., Peng, J. F., Shang, D. J., Zheng, J., Du, Z. F., Wu, Z., Shao,
641 M., Zeng, L. M., Molina, M. J., and Zhang, R. Y.: Elucidating severe urban haze
642 formation in China, Proceedings of the National Academy of Sciences of the United
643 States of America, 111, 17373-17378, 10.1073/pnas.1419604111, 2014.

644 Guo, S., Hu, M., Wang, Z. B., Slanina, J., and Zhao, Y. L.: Size-resolved aerosol
645 water-soluble ionic compositions in the summer of Beijing: implication of regional
646 secondary formation, Atmospheric Chemistry and Physics, 10, 947-959, 2010.

647 Hong, S.-Y., and Lim, J.-O. J.: The WRF Single-Moment 6-Class Microphysics Scheme
648 (WSM6), Asia-Pacific Journal of Atmospheric Sciences, 42, 129-151, 2006.

649 Horowitz, L. W., Walters, S., Mauzerall, D. L., Emmons, L. K., Rasch, P. J., Granier, C., Tie,
650 X. X., Lamarque, J. F., Schultz, M. G., Tyndall, G. S., Orlando, J. J., and Brasseur, G. P.:
651 A global simulation of tropospheric ozone and related tracers: Description and evaluation
652 of MOZART, version 2, Journal of Geophysical Research-Atmospheres, 108, 29,
653 10.1029/2002jd002853, 2003.

654 Janjić, Z. I.: Nonsingular Implementation of the Mellor–Yamada Level 2.5 Scheme in the
655 NCEP Meso Model, Ncep Office Note, 436, 2002.

656 Jiang, C., Wang, H., Zhao, T., Li, T., and Che, H.: Modeling study of $PM_{2.5}$ pollutant
657 transport across cities in China's Jing-Jin-Ji region during a severe haze episode in
658 December 2013, Atmospheric Chemistry and Physics, 15, 5803-5814,
659 10.5194/acp-15-5803-2015, 2015.

660 Jiang, F., Wang, T. J., Wang, T. T., Xie, M., and Zhao, H.: Numerical modeling of a
661 continuous photochemical pollution episode in Hong Kong using WRF-Chem,
662 Atmospheric Environment, 42, 8717-8727, 10.1016/j.atmosenv.2008.08.034, 2008.

663 Kulmala, M., Laaksonen, A., and Pirjola, L.: Parameterizations for sulfuric acid/water
664 nucleation rates, Journal of Geophysical Research-Atmosphere, 103, 8301– 8307, 1998.

665 Lang, J. L., Cheng, S. Y., Li, J. B., Chen, D. S., Zhou, Y., Wei, X., Han, L. H., and Wang, H.
666 Y.: A Monitoring and Modeling Study to Investigate Regional Transport and
667 Characteristics of PM2.5 Pollution, Aerosol and Air Quality Research, 13, 943-956,
668 10.4209/aaqr.2012.09.0242, 2013.

669 Lei, W., de Foy, B., Zavala, M., Volkamer, R., and Molina, L. T.: Characterizing ozone
670 production in the Mexico City Metropolitan Area: a case study using a chemical transport
671 model, Atmospheric Chemistry and Physics, 7, 1347-1366, 2007.

672 Lei, W., Zavala, M., de Foy, B., Volkamer, R., and Molina, L. T.: Characterizing ozone
673 production and response under different meteorological conditions in Mexico City,
674 Atmospheric Chemistry and Physics, 8, 7571-7581, 2008.

675 Long, X., Tie, X., Cao, J., Huang, J., Feng, T., Li, N., Zhao, S., Tian, J., Li, G., and Zhang, Q.:
676 Impact of crop field burning and mountains on heavy haze in the North China Plain: a

677 case study, Atmospheric Chemistry and Physics, 16, 9675-9691,
678 doi:10.5194/acp-16-9675-2016, 2016.

679 Li, G., Zhang, R., Fan, J., and Tie, X.: Impacts of black carbon aerosol on photolysis and
680 ozone, Journal of Geophysical Research, 110, 10.1029/2005jd005898, 2005.

681 Li, G., Zhang, R., Fan, J., and Tie, X.: Impacts of biogenic emissions on photochemical
682 ozone production in Houston, Texas, Journal of Geophysical Research, 112,
683 10.1029/2006jd007924, 2007.

684 Li, G., Lei, W., Zavala, M., Volkamer, R., Dusanter, S., Stevens, P., and Molina, L. T.:
685 Impacts of HONO sources on the photochemistry in Mexico City during the
686 MCMA-2006/MILAGO Campaign, Atmospheric Chemistry and Physics, 10, 6551-6567,
687 10.5194/acp-10-6551-2010, 2010.

688 Li, G., Bei, N., Tie, X., and Molina, L. T.: Aerosol effects on the photochemistry in Mexico
689 City during MCMA-2006/MILAGRO campaign, Atmospheric Chemistry and Physics, 11,
690 5169-5182, 10.5194/acp-11-5169-2011, 2011a.

691 Li, G., Zavala, M., Lei, W., Tsimpidi, A. P., Karydis, V. A., Pandis, S. N., Canagaratna, M.
692 R., and Molina, L. T.: Simulations of organic aerosol concentrations in Mexico City using
693 the WRF-CHEM model during the MCMA-2006/MILAGRO campaign, Atmospheric
694 Chemistry and Physics, 11, 3789-3809, 10.5194/acp-11-3789-2011, 2011b.

695 Li, G., Lei, W., Bei, N., and Molina, L. T.: Contribution of garbage burning to chloride and
696 PM2.5 in Mexico City, Atmospheric Chemistry and Physics, 12, 8751-8761,
697 10.5194/acp-12-8751-2012, 2012.

698 Li, G. H., Bei, N. F., Zavala, M., and Molina, L. T.: Ozone formation along the California
699 Mexican border region during Cal-Mex 2010 field campaign, Atmospheric Environment,
700 88, 370-389, 10.1016/j.atmosenv.2013.11.067, 2014.

701 Li, G., Bei, N., Cao, J., Huang, R., Wu, J., Feng, T., Wang, Y., Liu, S., Zhang, Q., Tie, X.,
702 and Molina, L.: A Possible Pathway for Rapid Growth of Sulfate during Haze Days in
703 China, Atmospheric Chemistry and Physics Discussion, 2016, 1-43,
704 10.5194/acp-2016-994, 2016.

705 Li, R. K., Li, Z. P., Gao, W. J., Ding, W. J., Xu, Q., and Song, X. F.: Diurnal, seasonal, and
706 spatial variation of $PM_{2.5}$ in Beijing, Chinese Science Bulletin, 60, 387-395,
707 10.1007/s11434-014-0607-9, 2015a.

708 Liu, Z. R., Hu, B., Wang, L. L., Wu, F. K., Gao, W. K., and Wang, Y. S.: Seasonal and
709 diurnal variation in particulate matter (PM_{10} and $PM_{2.5}$) at an urban site of Beijing:
710 analyses from a 9-year study, Environmental Science and Pollution Research, 22,
711 627-642, 10.1007/s11356-014-3347-0, 2015.

712 Meng, W., Gao, Q., Zhang, Z., Liao, Q., Lei, t., Li, J., Kang, N., and Ren, Z.: The Numerical
713 Study of Atmospheric Pollution in Beijing and Its Surrounding Regions, Research of
714 Environmental Sciences, 19, 11-18, 2006.

715 Mlawer, E. J., Taubman, S. J., Brown, P. D., Iacono, M. J., and Clough, S. A.: Radiative
716 transfer for inhomogeneous atmospheres: RRTM, a validated correlated-k model for the

longwave, Journal of Geophysical Research-Atmospheres, 102, 16663-16682, 10.1029/97jd00237, 1997.

Nenes, A., Pilinis, C., Pandis, S. N.: ISORROPIA: A New thermodynamic equilibrium model for multiphase multicomponent inorganic aerosols, Aquatic Geochemistry, 4(1), 123-152, http://nenes.eas.gatech.edu/ISORROPIA/, 1998.

Parrish, D. and Zhu, T.: Clean air for Megacities, Science, 326, 674-675, 2009.

Peng, J. F., Hu, M., Guo, S., Du, Z. F., Zheng, J., Shang, D. J., Zamora, M. L., Zeng, L. M., Shao, M., Wu, Y. S., Zheng, J., Wang, Y., Glen, C. R., Collins, D. R., Molina, M. J., and Zhang, R. Y.: Markedly enhanced absorption and direct radiative forcing of black carbon under polluted urban environments, Proceedings of the National Academy of Sciences of the United States of America, 113, 4266-4271, 10.1073/pnas.1602310113, 2016.

Sillman, S., Logan, J. A., and Wofsy, S. C.: The sensitivity of ozone to nitrogen oxides and hydrocarbons in regional ozone episode, Journal of Geophysical Research-Atmospheres, 95, 1837-1851, 10.1029/JD095iD02p01837, 1990.

Stein, U., and Alpert, P.: Factor separation in numerical simulations, J. Atmos. Sci., 50, 2107-2115, 10.1175/1520-0469(1993) 050<2107:fsins>2.0.co;2, 1993.

Streets, D. G., Fu, J. S., Jang, C. J., Hao, J. M., He, K. B., Tang, X. Y., Zhang, Y. H., Wang, Z. F., Li, Z. P., Zhang, Q., Wang, L. T., Wang, B. Y., and Yu, C.: Air quality during the 2008 Beijing Olympic Games, Atmospheric Environment, 41, 480-492, 10.1016/j.atmosenv.2006.08.046, 2007.

Suarex, M. J., and Chou, M. D.: Technical report series on global modeling and data assimilation. Volume 3: An efficient thermal infrared radiation parameterization for use in general circulation models, 1603-1609, 1994.

Suh, I., Zhang, R. Y., Molina, L. T., and Molina, M. J.: Oxidation mechanism of aromatic peroxy and bicyclic radicals from OH-toluene reactions, Journal of American Chemical Society, 125, 12655-12665, 10.1021/ja0350280, 2003.

Sun, Y. L., Jiang, Q., Wang, Z. F., Fu, P. Q., Li, J., Yang, T., and Yin, Y.: Investigation of the sources and evolution processes of severe haze pollution in Beijing in January 2013, Journal of Geophysical Research-Atmospheres, 119, 4380-4398, 10.1002/2014jd021641, 2014.

Tang, G., Li, X., Wang, Y., Xin, J., and Ren, X.: Surface ozone trend details and interpretations in Beijing, 2001-2006, Atmospheric Chemistry and Physics, 9, 8813-8823, 2009.

Tang, G., Wang, Y., Li, X., Ji, D., Hsu, S., and Gao, X.: Spatial-temporal variations in surface ozone in Northern China as observed during 2009-2010 and possible implications for future air quality control strategies, Atmospheric Chemistry and Physics, 12, 2757-2776, 10.5194/acp-12-2757-2012, 2012.

Tang, G. Q., Zhang, J. Q., Zhu, X. W., Song, T., Munkel, C., Hu, B., Schafer, K., Liu, Z. R., Zhang, J. K., Wang, L. L., Xin, J. Y., Suppan, P., and Wang, Y. S.: Mixing layer height and its implications for air pollution over Beijing, China, Atmospheric Chemistry and

Physics, 16, 2459-2475, 10.5194/acp-16-2459-2016, 2016.

Tao, M. H., Chen, L. F., Xiong, X. Z., Zhang, M. G., Ma, P. F., Tao, J. H., and Wang, Z. F.: Formation process of the widespread extreme haze pollution over northern China in January 2013: Implications for regional air quality and climate, Atmospheric Environment, 98, 417-425, 10.1016/j.atmosenv.2014.09.026, 2014.

Volkamer, R., San Martini, F., Molina, L. T., Salcedo, D., Jimenez, J. L., and Molina, M. J.: A Missing Sink for Gas-Phase Glyoxal in Mexico City: Formation of Secondary Organic Aerosol, Geophysical Research Letter, 34, L19807, doi:10.1029/2007GL030752, 2007.

Wang, H., Xue, M., Zhang, X. Y., Liu, H. L., Zhou, C. H., Tan, S. C., Che, H. Z., Chen, B., and Li, T.: Mesoscale modeling study of the interactions between aerosols and PBL meteorology during a haze episode in Jing-Jin-Ji (China) and its nearby surrounding region - Part 1: Aerosol distributions and meteorological features, Atmospheric Chemistry and Physics, 15, 3257-3275, 10.5194/acp-15-3257-2015, 2015.

Wang, L. L., Liu, Z. R., Sun, Y., Ji, D. S., and Wang, Y. S.: Long-range transport and regional sources of $PM_{2.5}$ in Beijing based on long-term observations from 2005 to 2010, Atmospheric Research, 157, 37-48, 10.1016/j.atmosres.2014.12.003, 2015.

Wang, L. T., Wei, Z., Yang, J., Zhang, Y., Zhang, F. F., Su, J., Meng, C. C., and Zhang, Q.: The 2013 severe haze over southern Hebei, China: model evaluation, source apportionment, and policy implications, Atmospheric Chemistry and Physics, 14, 3151-3173, 10.5194/acp-14-3151-2014, 2014a.

Wang, X. S., Li, J. L., Zhang, Y. H., Xie, S. D., and Tang, X. Y.: Ozone source attribution during a severe photochemical smog episode in Beijing, China, Science of China Series B - Chemistry, 52, 1270-1280, 10.1007/s11426-009-0137-5, 2009.

Wang, Y., Khalizov, A., Levy, M., and Zhang, R. Y.: New Directions: Light absorbing aerosols and their atmospheric impacts, Atmospheric Environment, 81, 713-715, 10.1016/j.atmosenv.2013.09.034, 2013.

Wang, Y., Konopka, P., Liu, Y., Chen, H., Muller, R., Ploger, F., Riese, M., Cai, Z., and Lu, D.: Tropospheric ozone trend over Beijing from 2002-2010: ozonesonde measurements and modeling analysis, Atmospheric Chemistry and Physics, 12, 8389-8399, 10.5194/acp-12-8389-2012, 2012.

Wang, Y. H., Hu, B., Tang, G. Q., Ji, D. S., Zhang, H. X., Bai, J. H., Wang, X. K., and Wang, Y. S.: Characteristics of ozone and its precursors in Northern China: A comparative study of three sites, Atmospheric Research, 132, 450-459, 10.1016/j.atmosres.2013.04.005, 2013.

Wang, Z., Li, Y., Chen, T., Zhang, D., Sun, F., Wang, X., Huan, N., and Pan, L.: Analysis on diurnal variation characteristics of ozone and correlations with its precursors in urban atmosphere of Beijing, China Environmental Science, 34, 3001-3008, 2014b.

Wang, Z., Zhang, D., Li, Y., Dong, X., Sun, R., and Sun, N.: Different Air Pollution Situations of O_3 and $PM_{2.5}$ During Summer in Beijing, Environmental Science, 37, 807-815, 2016.

797 Wang, Z. F., Li-Na, L. I., Qi-Zhong, W. U., Gao, C., Xin, L. I., Student, G., and PhD:
798 Simulation of the Impacts of Regional Transport on Summer Ozone Levels Over Beijing,
799 Chinese Journal of Nature, 2008.

800 Weinroth, E., Luria, M., Emery, C., Ben-Nun, A., Bornstein, R., Kaplan, J., Peleg, M., and
801 Mahrer, Y.: Simulations of Mideast transboundary ozone transport: A source
802 apportionment case study, Atmospheric Environment, 42, 3700-3716,
803 10.1016/j.atmosenv.2008.01.002, 2008.

804 Wesely, M. L.: Parameterization of surface resistances to gaseous dry deposition in
805 regional-scale numerical models, Atmospheric Environment, 23, 1293-1304,
806 10.1016/0004-6981(89)90153-4, 1989.

807 Xie, Y. Y., Wang, Y. X., Zhang, K., Dong, W. H., Lv, B. L., and Bai, Y. Q.: Daily
808 Estimation of Ground-Level $PM_{2.5}$ Concentrations over Beijing Using 3 km Resolution
809 MODIS AOD, Environmental science & technology, 49, 12280-12288,
810 10.1021/acs.est.5b01413, 2015.

811 Yang, T., Wang, Z. F., Zhang, B., Wang, X. Q., Wang, W., Gbauidi, A., and Gong, Y. B.:
812 Evaluation of the effect of air pollution control during the Beijing 2008 Olympic Games
813 using Lidar data, Chinese Science Bulletin, 55, 1311-1316, 10.1007/s11434-010-0081-y,
814 2010.

815 Zhang, L., Liao, H., and Li, J. P.: Impacts of Asian summer monsoon on seasonal and
816 interannual variations of aerosols over eastern China, Journal of Geophysical
817 Research-Atmospheres, 115, 20, 10.1029/2009jd012299, 2010.

818 Zhang, J. P., Zhu, T., Zhang, Q. H., Li, C. C., Shu, H. L., Ying, Y., Dai, Z. P., Wang, X., Liu,
819 X. Y., Liang, A. M., Shen, H. X., and Yi, B. Q.: The impact of circulation patterns on
820 regional transport pathways and air quality over Beijing and its surroundings,
821 Atmospheric Chemistry and Physics, 12, 5031-5053, 10.5194/acp-12-5031-2012, 2012.

822 Zhang, Q., Streets, D. G., Carmichael, G. R., He, K. B., Huo, H., Kannari, A., Klimont, Z.,
823 Park, I. S., Reddy, S., Fu, J. S., Chen, D., Duan, L., Lei, Y., Wang, L. T., and Yao, Z. L.:
824 Asian emissions in 2006 for the NASA INTEX-B mission, Atmospheric Chemistry and
825 Physics, 9, 5131-5153, 2009.

826 Zhang, Q., Yuan, B., Shao, M., Wang, X., Lu, S., Lu, K., Wang, M., Chen, L., Chang, C. C.,
827 and Liu, S. C.: Variations of ground-level O_3 and its precursors in Beijing in summertime
828 between 2005 and 2011, Atmospheric Chemistry and Physics, 14, 6089-6101,
829 10.5194/acp-14-6089-2014, 2014.

830 Zhang, R., Jing, J., Tao, J., Hsu, S.-C., Wang, G., Cao, J., Lee, C. S. L., Zhu, L., Chen, Z.,
831 Zhao, Y., and Shen, Z.: Chemical characterization and source apportionment of $PM_{2.5}$ in
832 Beijing: seasonal perspective, Atmospheric Chemistry and Physics, 13, 7053-7074,
833 doi:10.5194/acp-13-7053-2013, 2013.

834 Zhang, R., Wang, L., Khalizova, A. F., Zhao, J., Zheng, J., Mc-Grawb, R. L., and Molina, L.
835 T.: Formation of nanoparticles of blue haze enhanced by anthropogenic pollution,
836 Proceedings of the National Academy of Sciences of the United States of America, 106,

17650–17654, 2009.

Zhang, R., Khalizova, A. F., Wang, L., Hu, M., and Xu, W.: Nucleation and growth of nanoparticles in the atmosphere, Chemical Reviews, 112, 1957–2011, 2012.

Zhang, R. Y., Wang, G. H., Guo, S., Zarnora, M. L., Ying, Q., Lin, Y., Wang, W. G., Hu, M., and Wang, Y.: Formation of Urban Fine Particulate Matter, Chemical Reviews, 115, 3803-3855, 10.1021/acs.chemrev.5b00067, 2015.

Zhao, J., Levitt, N. P., Zhang, R. Y., and Chen, J. M.: Heterogeneous reactions of methylglyoxal in acidic media: implications for secondary organic aerosol formation, Environment Science & Technology, 40, 7682–7687, 2006.

Zheng, S., Pozzer, A., Cao, C. X., and Lelieveld, J.: Long-term (2001-2012) concentrations of fine particulate matter ($PM_{2.5}$) and the impact on human health in Beijing, China, Atmospheric Chemistry and Physics, 15, 5715-5725, 10.5194/acp-15-5715-2015, 2015.

853 Table 1 Emissions of major anthropogenic species in July 2013 (Unit: 10^6 g $month^{-1}$)

854

Region	VOC	NO_x	OC	SO_2	CO	$PM_{2.5}$
Beijing Municipality	29303	26272	976	8796	119254	5319
Tianjin Municipality	29255	34534	1424	23204	181940	8831
Hebei Province	101710	190352	12732	136957	1239510	67877
Shanxi Province	35933	93069	6381	131758	355823	36473
Shandong Province	246538	235485	12181	246538	937528	77681

855

856

857

858

859

860

Table 2 Hourly mass concentrations of pollutants averaged in the afternoon at 12 monitoring sites in Beijing during summertime of 2013 and 2015.

Pollutants	CO (mg m^{-3})	SO_2 (μg m^{-3})	NO_2 (μg m^{-3})	O_3 (μg m^{-3})	$PM_{2.5}$ (μg m^{-3})
2013	1.09	9.85	31.6	133.0	81.4
2015	0.88	5.71	23.6	163.2	61.9
Change (%)	-20.0	-42.0	-25.1	+22.8	-24.0

Table 3 Average O_3 contributions (%) from 12：00 to 18:00 BJT in Beijing from only-Beijing emissions, non-Beijing emissions, the interactions of both emissions, and background from 5 to 14 July 2015.

Emissions	Beijing	Surroundings	Interactions	Background
Date	f'_B	f'_S	f'_{BS}	f_0
5	15.5	26.1	-2.4	60.8
6	19.8	30.9	-3.0	52.3
7	25.5	36.0	-3.6	42.1
8	27.0	36.9	-5.9	42.0
9	23.2	35.3	-4.6	46.1
10	18.6	39.9	-2.6	44.1
11	29.4	48.0	-10.0	32.6
12	35.4	40.6	-11.4	35.4
13	23.4	15.2	-1.5	62.9
14	20.3	32.2	-3.3	50.8
Average	22.4	36.6	-5.1	46.1

877 Table 4 Average $PM_{2.5}$ contributions (%) in Beijing from only-Beijing emissions,
878 non-Beijing emissions, the interactions of both emissions, and background from 5 to 14 July
879 2015.
880

Emissions	Beijing	Surroundings	Interactions	Background
Date	f'_B	f'_S	f'_{BS}	f_0
5	14.6	55.1	3.3	27.0
6	14.9	56.3	3.4	25.4
7	14.2	56.4	8.0	21.4
8	13.2	61.1	6.4	19.3
9	15.3	61.3	6.3	17.1
10	11.5	66.5	6.2	15.8
11	9.7	71.0	8.1	11.2
12	14.2	67.6	5.6	12.6
13	19.2	47.2	3.6	30.0
14	16.6	53.1	6.4	23.9
Average	13.7	61.5	5.9	18.9

881
882
883
884
885

886 Table 5 Aerosol species' contributions (%) from only-Beijing emissions, non-Beijing
887 emissions, interactions of both emissions, and background, and mass fraction in the total
888 $PM_{2.5}$ (%) in Beijing averaged during the period from 5 to 14 July 2015.
889

Emissions Species	Mass Fraction In Total $PM_{2.5}$	Beijing f'_B	Surroundings f'_S	Interactions f'_{BS}	Background f_0
EC	5.8	27.0	57.9	1.5	13.6
POA	9.8	20.8	49.0	5.3	24.9
SOA	25.0	14.6	64.2	5.9	15.3
Ammonium	13.7	14.5	65.7	1.5	18.3
Nitrate	14.1	10.1	71.7	18.1	0.1
Sulfate	25.1	6.5	52.9	3.4	37.2
Unspecified	6.5	21.2	61.4	1.6	15.8

890
891
892
893

Figure Captions

Figure 1 WRF-CHEM simulation domain. The blue circles represent centers of cities with ambient monitoring sites and the red circle denotes the NCNST site. The size of the blue circle denotes the number of ambient monitoring sites of cities.

Figure 2 Spatial distributions of anthropogenic (a) NO_x, (b) VOCs, (c) OC, (d) SO_2 emission rates (g $month^{-1}$) in the simulation domain.

Figure 3 Comparison of measured (black dots) and predicted (blue line) diurnal profiles of near-surface hourly (a) $PM_{2.5}$, (b) O_3, and (c) NO_2 averaged over all ambient monitoring stations in Beijing from 5 to 14 July 2015.

Figure 4 Comparison of measured (black dots) and simulated (black line) diurnal profiles of submicron aerosol species of (a) POA, (b) SOA, (c) sulfate, (d) nitrate, and (e) ammonium at NCNST site in Beijing from 5 to 14 July 2015.

Figure 5 Comparison of measured (black dots) and predicted (blue line) diurnal profiles of near-surface hourly (a) $PM_{2.5}$, (b) O_3, and (c) NO_2 averaged over all ambient monitoring stations in BTH from 5 to 14 July 2015.

Figure 6 Pattern comparison of simulated vs. observed near-surface $PM_{2.5}$ at 10:00 BJT during the selected periods from 5 to 14 July 2015. Colored circles: $PM_{2.5}$ observations; color contour: $PM_{2.5}$ simulations; black arrows: simulated surface winds.

Figure 7 Same as Figure 6, but for O_3 at 15:00 BJT.

Figure 8 Same as Figure 6, but for NO_2 at 08:00 BJT.

Figure 9 Temporal variations of the total net horizontal transport flux of (a) $PM_{2.5}$, (b) O_3, and (c) NO_2 across Beijing boundary (blue line) and the contribution of non-Beijing emission to the $PM_{2.5}$, O_3, and NO_2 concentrations in Beijing (black line) from 5 to 14 July 2015.

Figure 10 Temporal variations of the average near-surface (a) O_3 and (b) $PM_{2.5}$ concentrations from $\boldsymbol{f_{BS}}$ with all the emissions (black line), $\boldsymbol{f_B}$ with Beijing emissions alone (blue line), and $\boldsymbol{f_S}$ with non-Beijing emissions alone (red line) in Beijing from 5 to 14 July 2015.

Figure 11 Temporal variations of the average contributions to the near-surface aerosol species concentrations from total emissions (black line, defined as $\boldsymbol{f_{BS}}$), only-Beijing emissions (blue line, $\boldsymbol{f'_B}$, defined as $\boldsymbol{f_B - f_0}$), non-Beijing emissions (red line, $\boldsymbol{f'_S}$, defined as $\boldsymbol{f_S - f_0}$), the emission interactions (green line, $\boldsymbol{f'_{BS}}$,

938 defined as $\boldsymbol{f_{BS} - f_B - f_S + f_0}$), and background (black dashed line, defined as
939 $\boldsymbol{f_0}$) in Beijing from 5 to 14 July 2015.
940
941
942
943

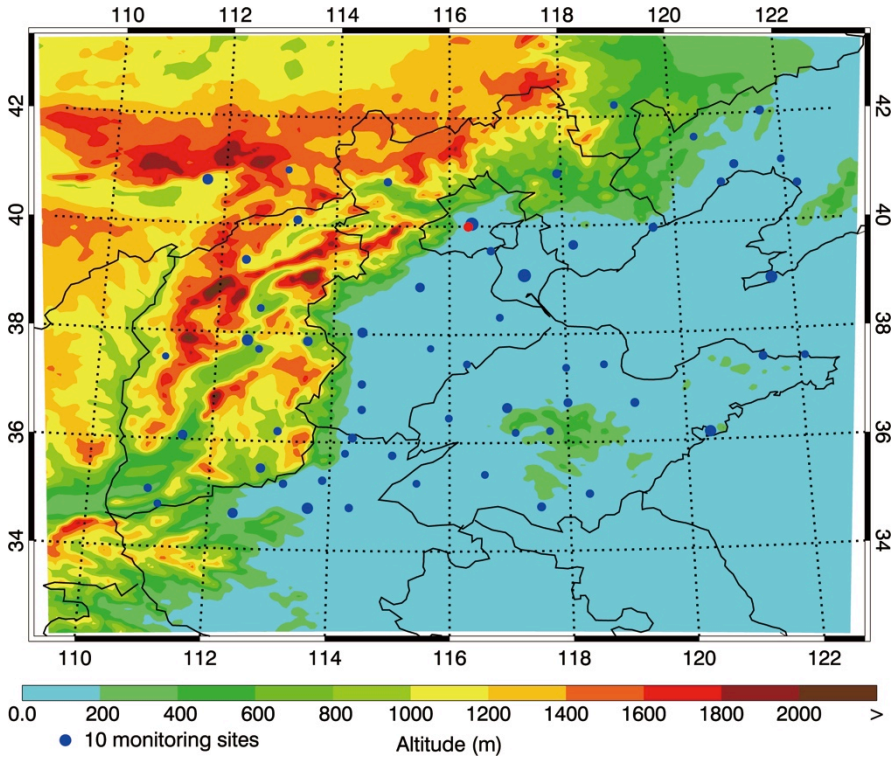
110
112
114
116
118
120
122
42
40
38
36
34
0.0
200
400
600
800
1000
1200
1400
1600
1800
2000
>
10 monitoring sites
Altitude (m)

Figure 1

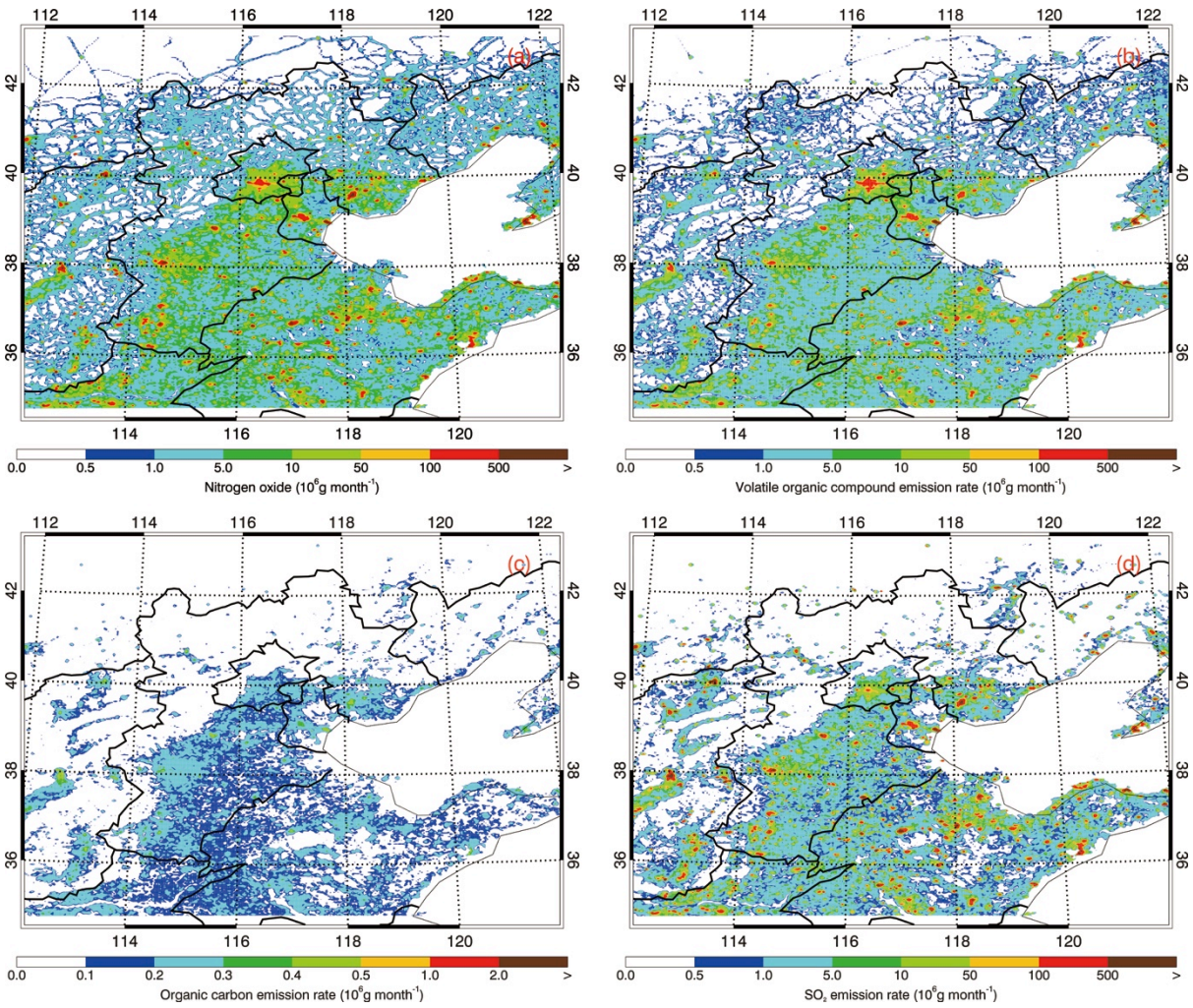
(a)
(b)
(c)
(d)
112 114 116 118 120 122
42 40 38 36
0.0 0.5 1.0 5.0 10 50 100 500 >
Nitrogen oxide (10^6g month^{-1})
Volatile organic compound emission rate (10^6g month^{-1})
0.0 0.1 0.2 0.3 0.4 0.5 1.0 2.0 >
Organic carbon emission rate (10^6g month^{-1})
0.0 0.5 1.0 5.0 10 50 100 500 >
SO_2 emission rate (10^6g month^{-1})

Figure 2

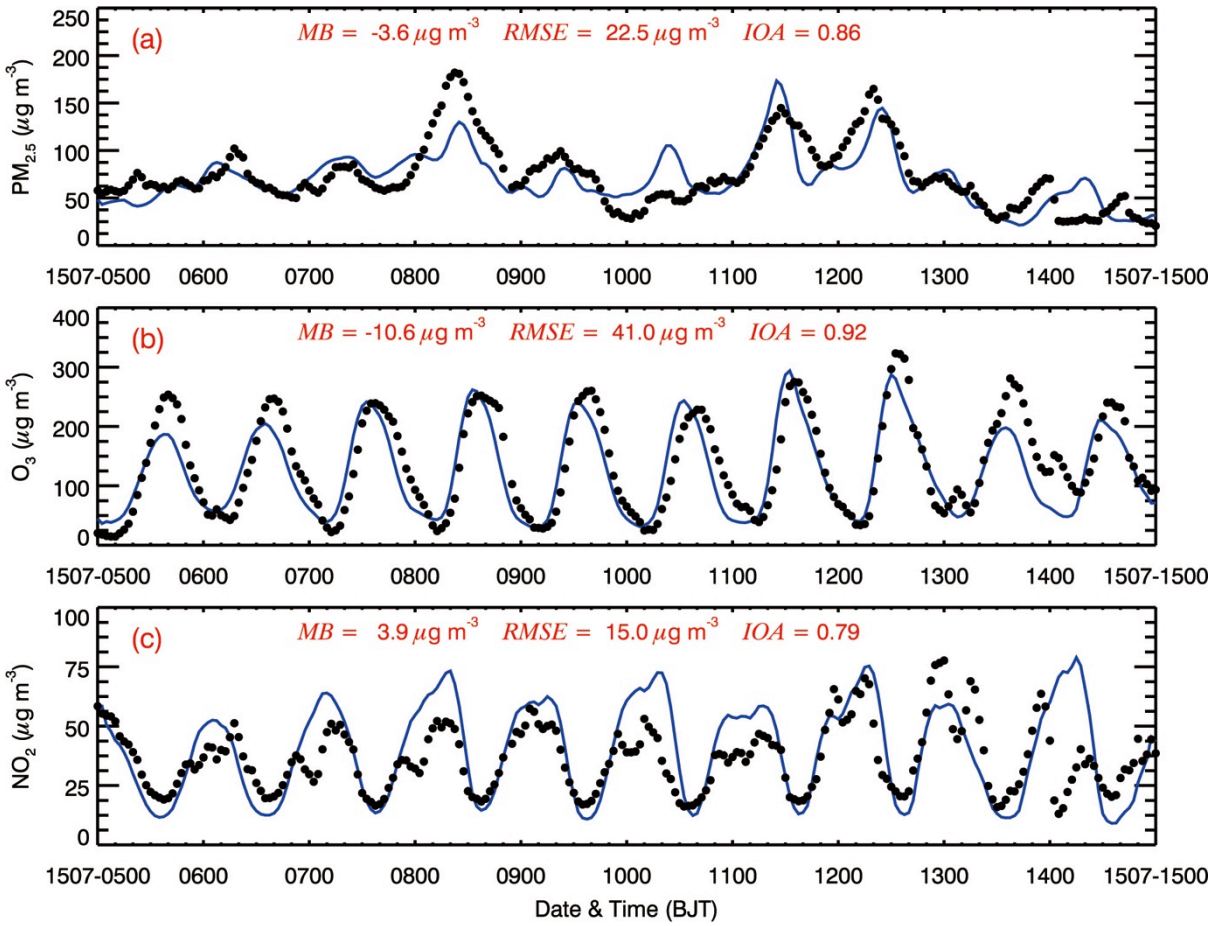
(a)
MB = -3.6 μg m-3 RMSE = 22.5 μg m-3 IOA = 0.86
PM2.5 (μg m-3)
(b)
MB = -10.6 μg m-3 RMSE = 41.0 μg m-3 IOA = 0.92
O3 (μg m-3)
(c)
MB = 3.9 μg m-3 RMSE = 15.0 μg m-3 IOA = 0.79
NO2 (μg m-3)
1507-0500 0600 0700 0800 0900 1000 1100 1200 1300 1400 1507-1500
Date & Time (BJT)

Figure 3

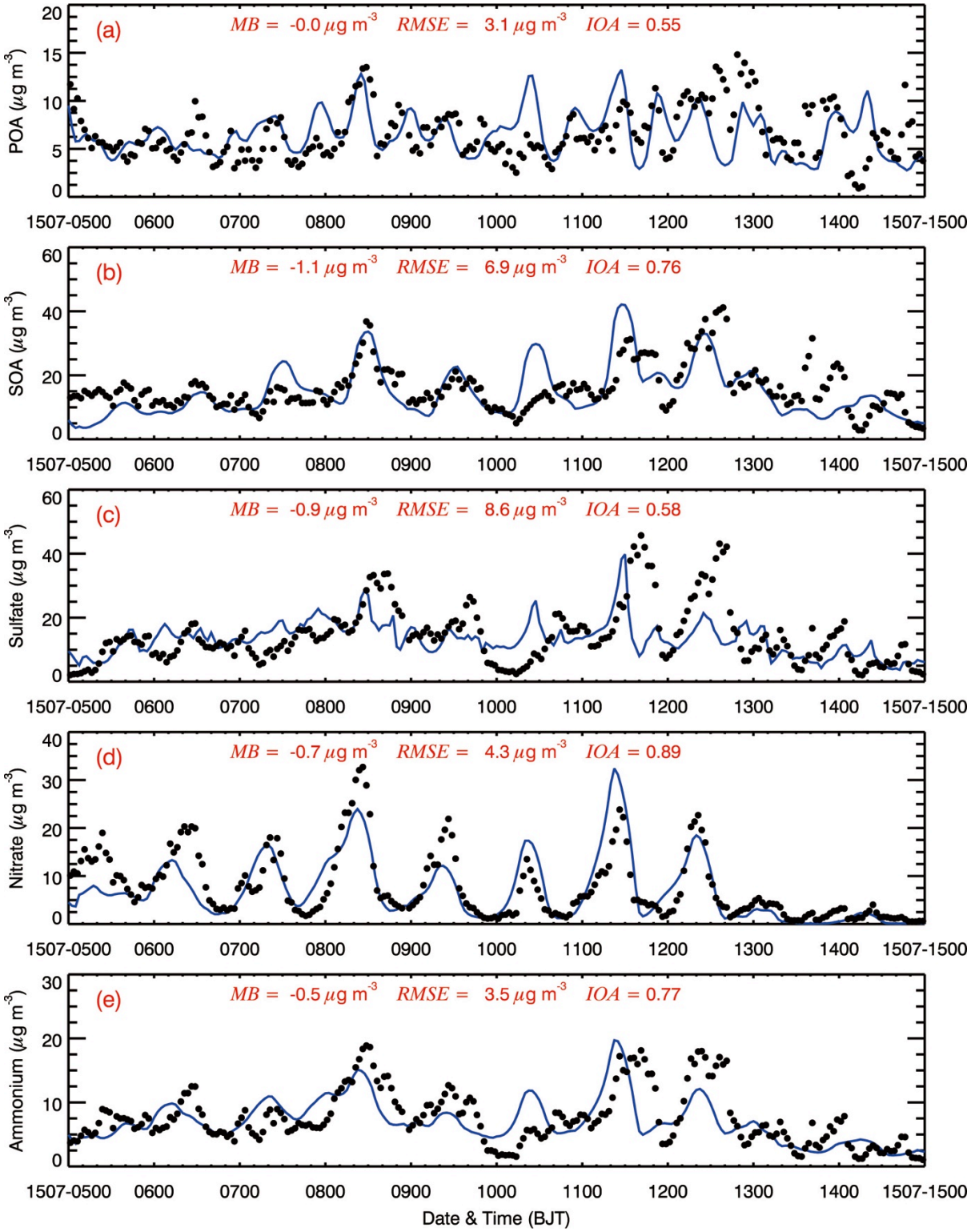
(a)
MB = -0.0 μg m-3 RMSE = 3.1 μg m-3 IOA = 0.55
POA (μg m-3)
(b)
MB = -1.1 μg m-3 RMSE = 6.9 μg m-3 IOA = 0.76
SOA (μg m-3)
(c)
MB = -0.9 μg m-3 RMSE = 8.6 μg m-3 IOA = 0.58
Sulfate (μg m-3)
(d)
MB = -0.7 μg m-3 RMSE = 4.3 μg m-3 IOA = 0.89
Nitrate (μg m-3)
(e)
MB = -0.5 μg m-3 RMSE = 3.5 μg m-3 IOA = 0.77
Ammonium (μg m-3)
1507-0500 0600 0700 0800 0900 1000 1100 1200 1300 1400 1507-1500
Date & Time (BJT)

Figure 4

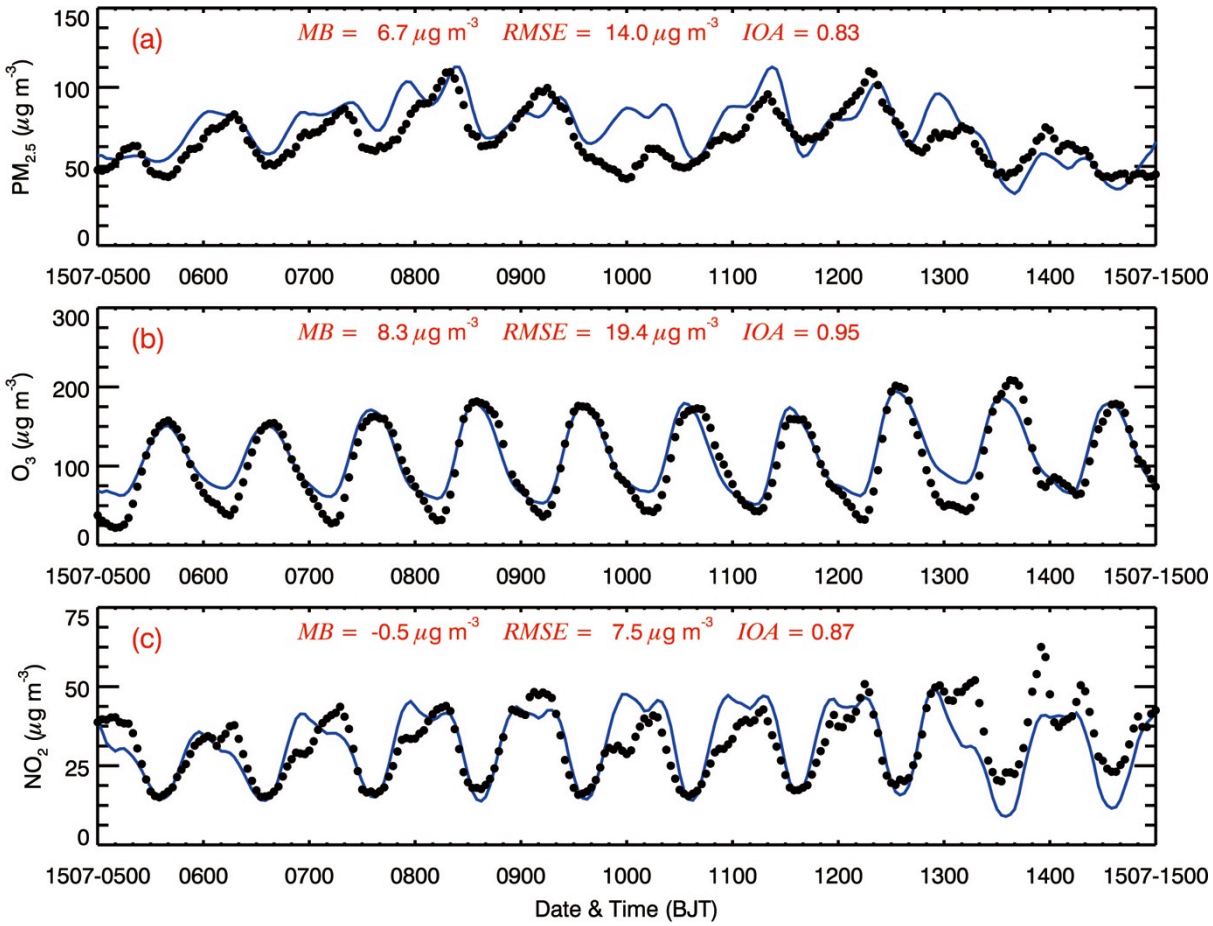
(a)
MB = 6.7 μg m-3 RMSE = 14.0 μg m-3 IOA = 0.83
PM2.5 (μg m-3)
150
100
50
0
(b)
MB = 8.3 μg m-3 RMSE = 19.4 μg m-3 IOA = 0.95
O3 (μg m-3)
300
200
100
0
(c)
MB = -0.5 μg m-3 RMSE = 7.5 μg m-3 IOA = 0.87
NO2 (μg m-3)
75
50
25
0
1507-0500 0600 0700 0800 0900 1000 1100 1200 1300 1400 1507-1500
Date & Time (BJT)

Figure 5

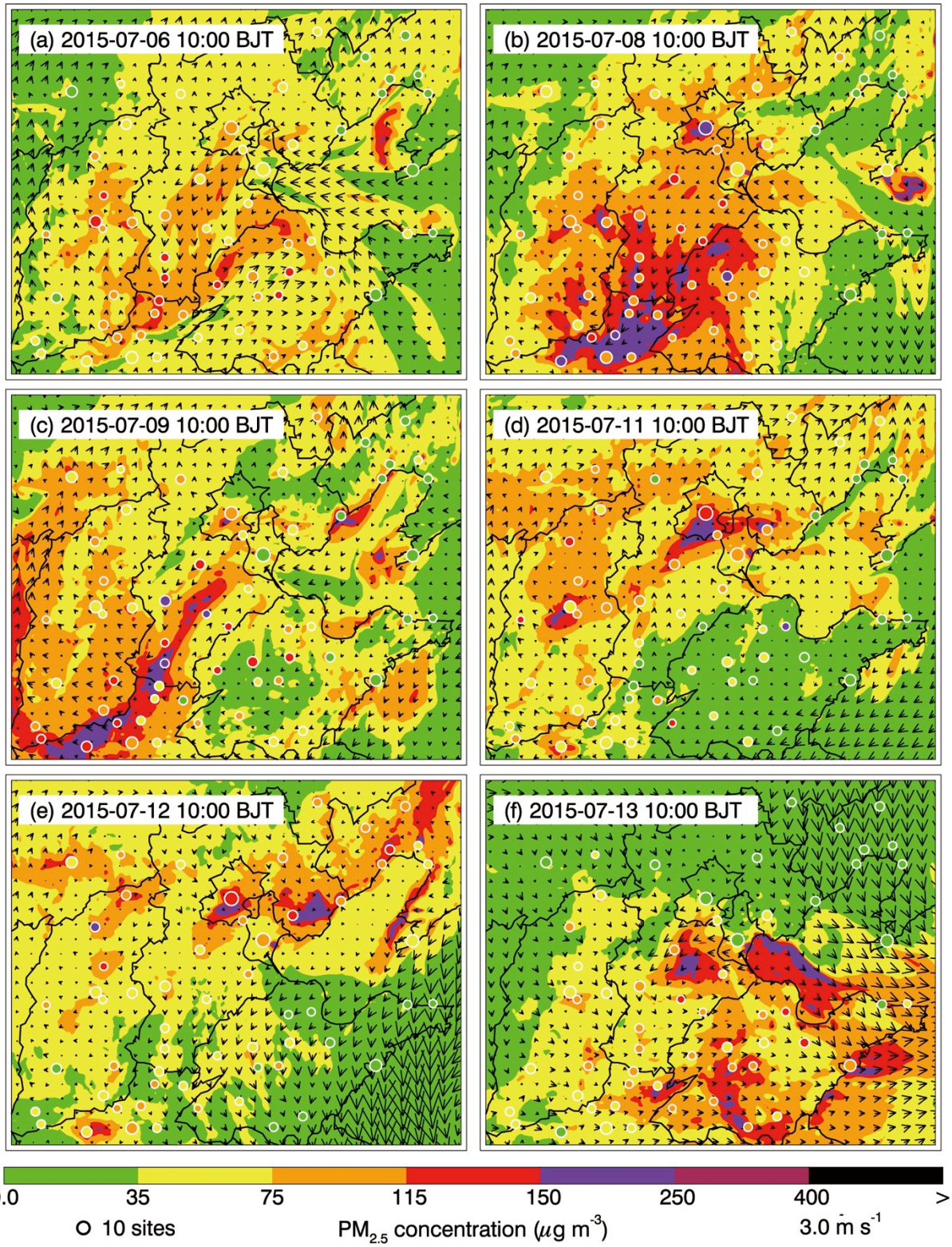
(a) 2015-07-06 10:00 BJT
(b) 2015-07-08 10:00 BJT
(c) 2015-07-09 10:00 BJT
(d) 2015-07-11 10:00 BJT
(e) 2015-07-12 10:00 BJT
(f) 2015-07-13 10:00 BJT
0.0
35
75
115
150
250
400
>
10 sites
PM2.5 concentration (μg m-3)
3.0 m s-1

Figure 6

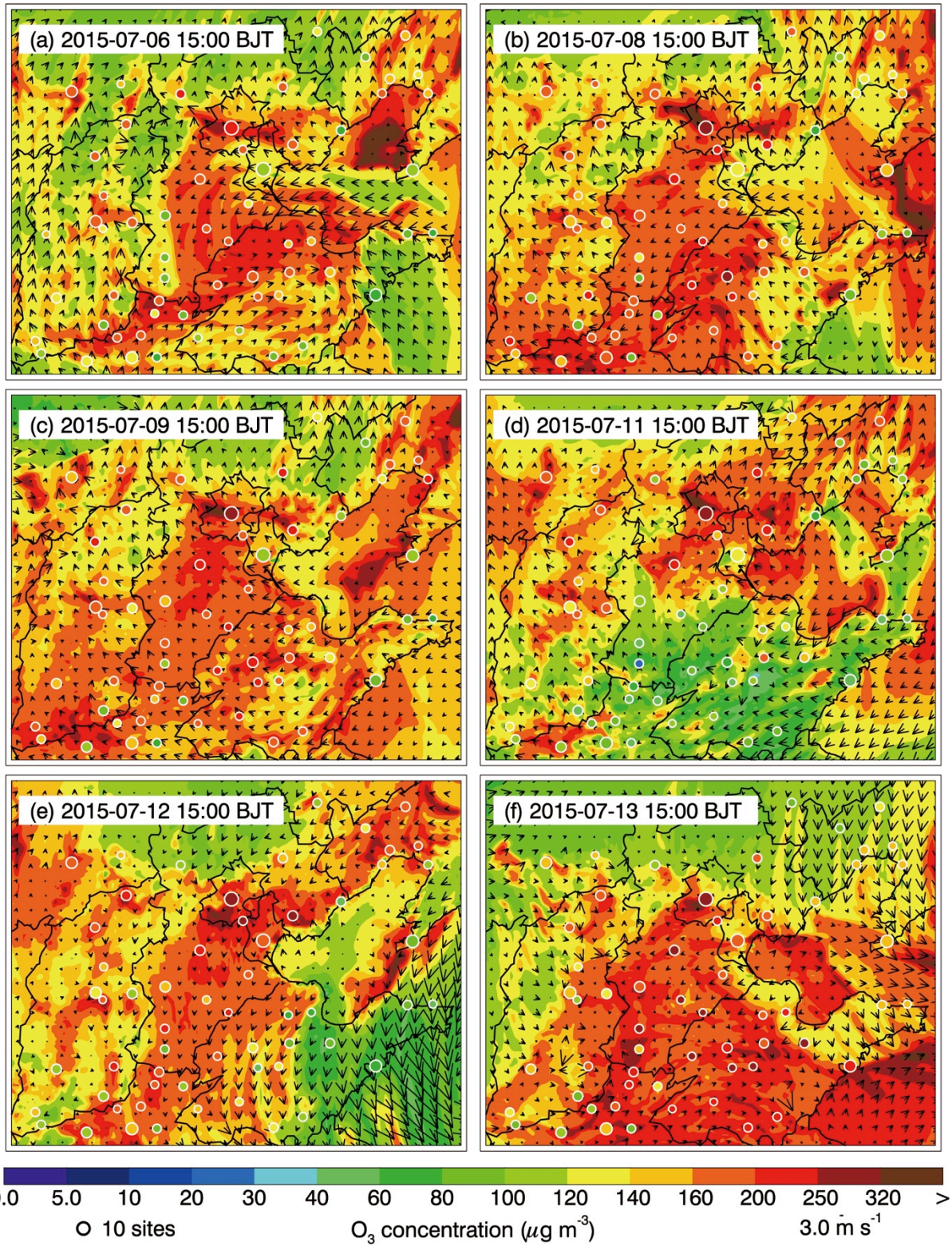
(a) 2015-07-06 15:00 BJT
(b) 2015-07-08 15:00 BJT
(c) 2015-07-09 15:00 BJT
(d) 2015-07-11 15:00 BJT
(e) 2015-07-12 15:00 BJT
(f) 2015-07-13 15:00 BJT
0.0 5.0 10 20 30 40 60 80 100 120 140 160 200 250 320 >
O 10 sites
O3 concentration (μg m-3)
3.0 m s-1

Figure 7

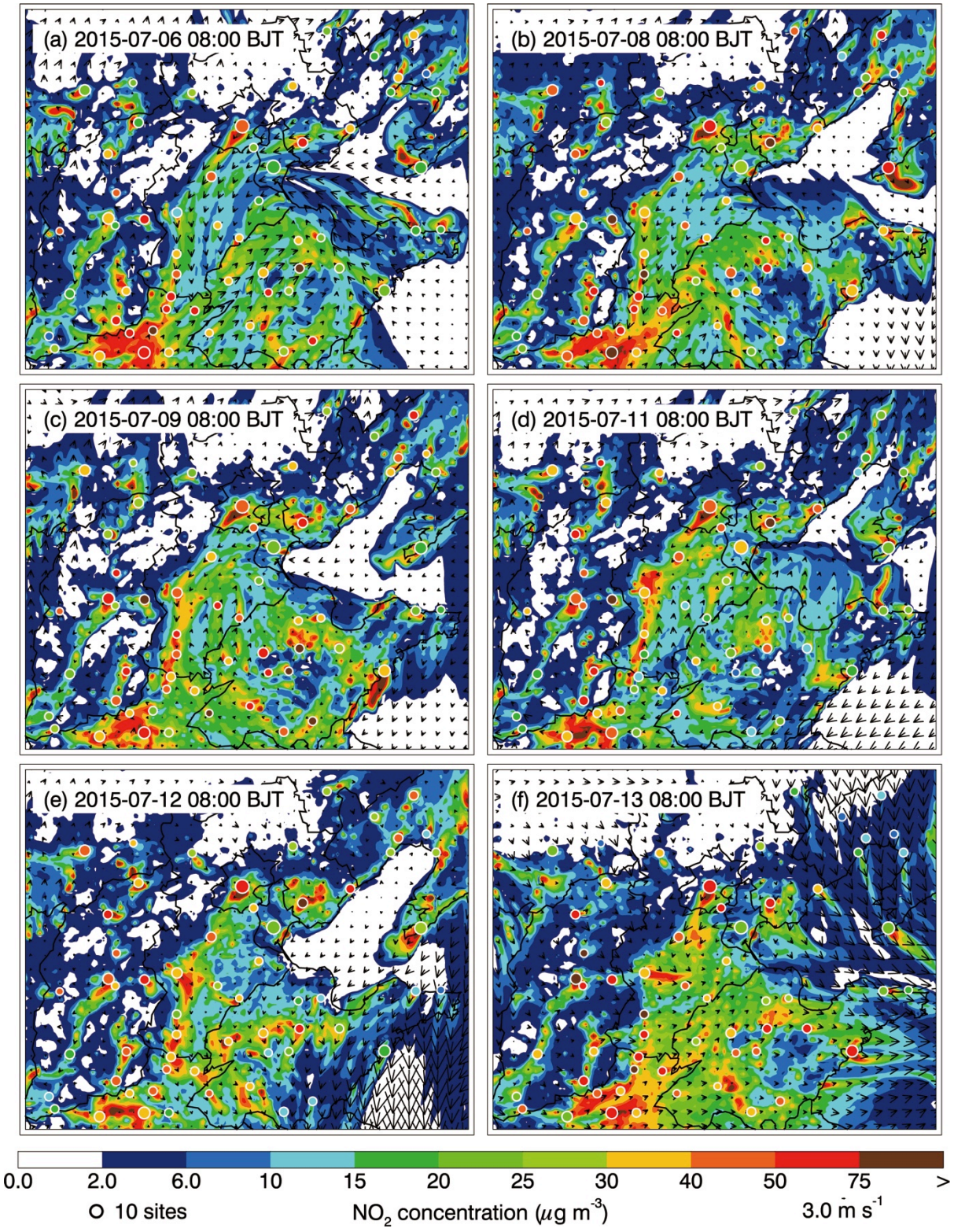
(a) 2015-07-06 08:00 BJT
(b) 2015-07-08 08:00 BJT
(c) 2015-07-09 08:00 BJT
(d) 2015-07-11 08:00 BJT
(e) 2015-07-12 08:00 BJT
(f) 2015-07-13 08:00 BJT
0.0
2.0
6.0
10
15
20
25
30
40
50
75
>
O 10 sites
NO2 concentration (μg m-3)
3.0 m s-1

Figure 8

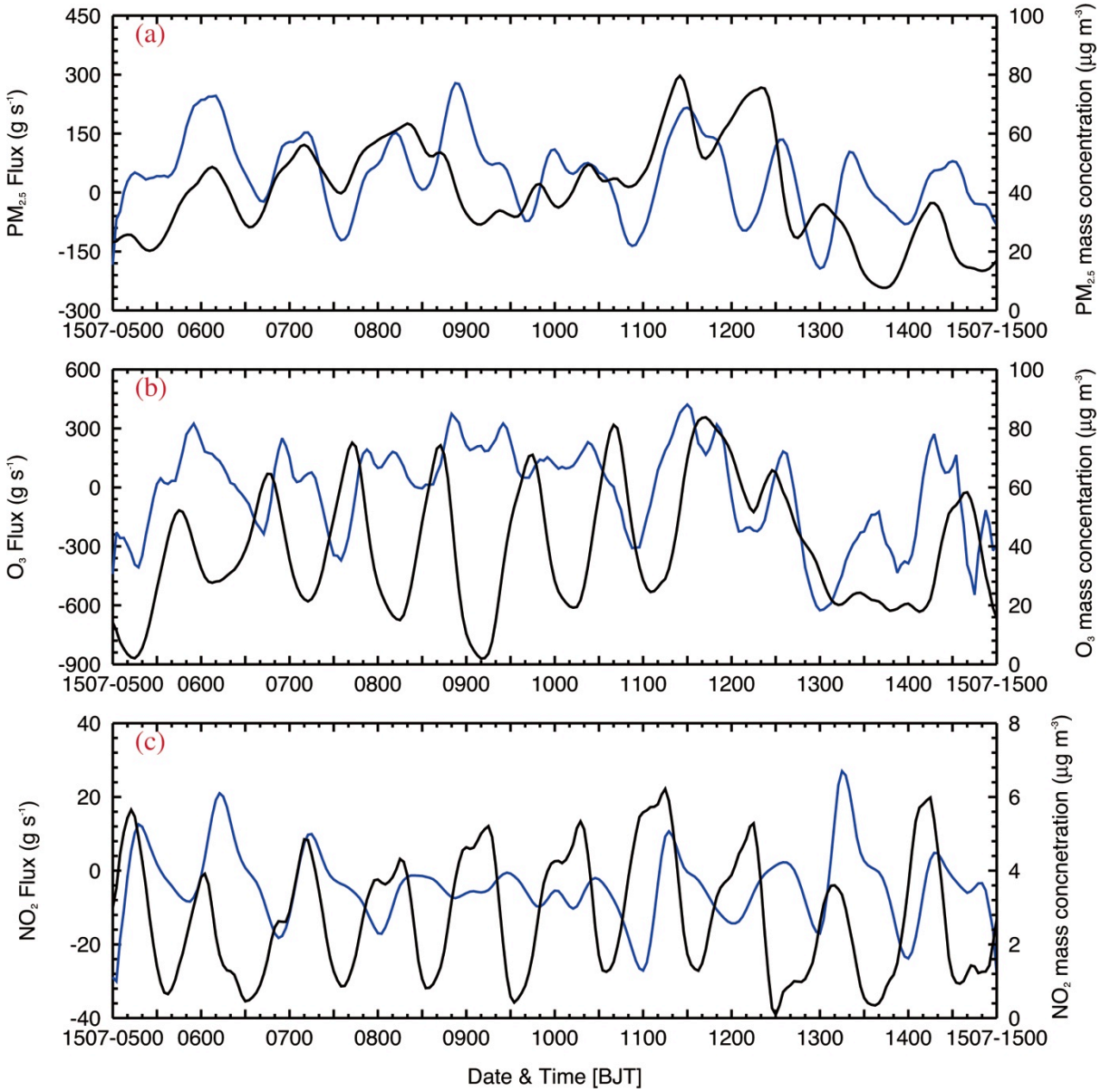
(a)
(b)
(c)
PM2.5 Flux (g s-1)
PM2.5 mass concentration (μg m-3)
O3 Flux (g s-1)
O3 mass concentartion (μg m-3)
NO2 Flux (g s-1)
NO2 mass concnetration (μg m-3)
1507-0500 0600 0700 0800 0900 1000 1100 1200 1300 1400 1507-1500
Date & Time [BJT]

Figure 9

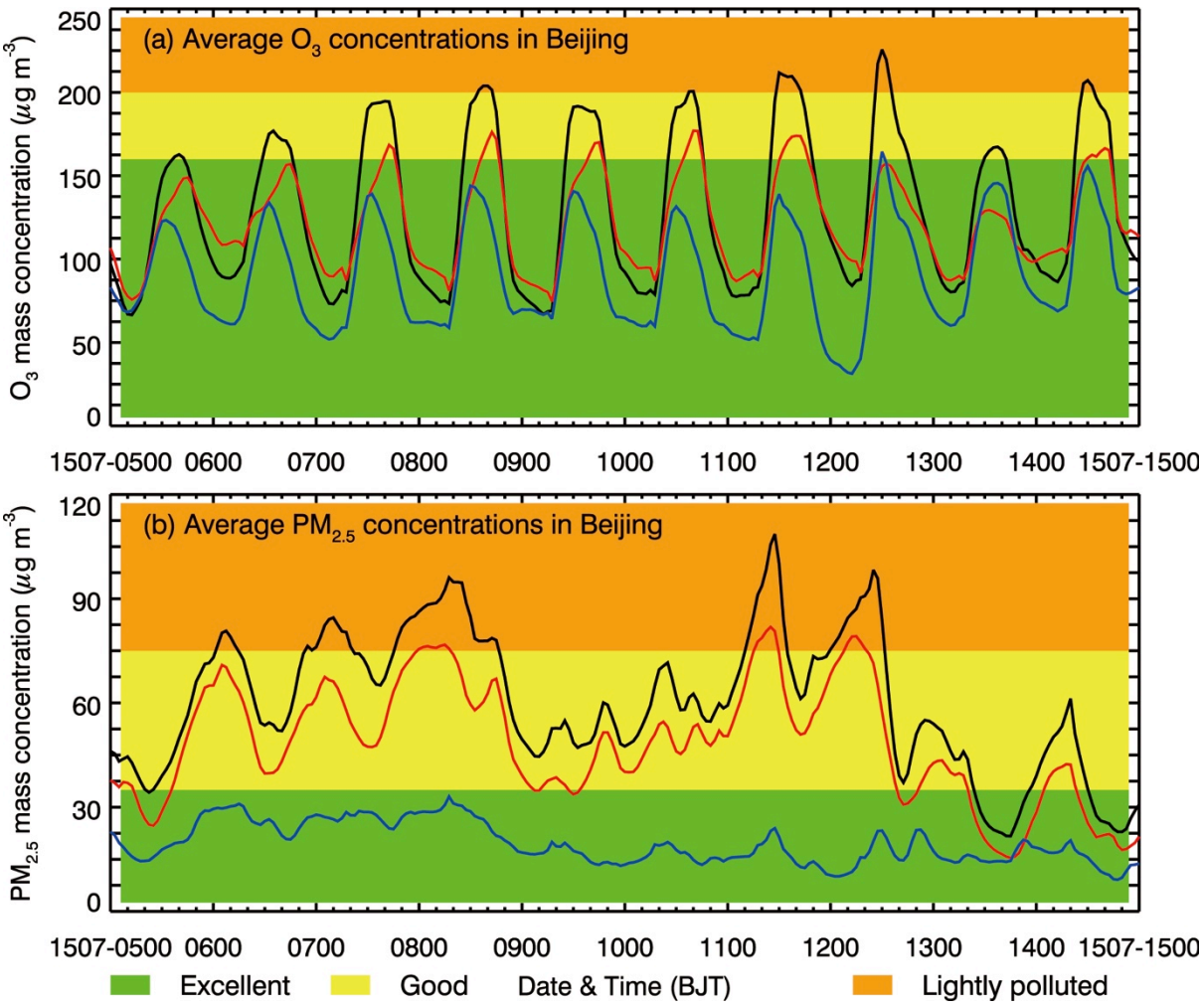
(a) Average O_3 concentrations in Beijing
O_3 mass concentration (μg m^{-3})
250
200
150
100
50
0
1507-0500
0600
0700
0800
0900
1000
1100
1200
1300
1400
1507-1500
(b) Average $PM_{2.5}$ concentrations in Beijing
$PM_{2.5}$ mass concentration (μg m^{-3})
120
90
60
30
0
Excellent
Good
Date & Time (BJT)
Lightly polluted

Figure 10

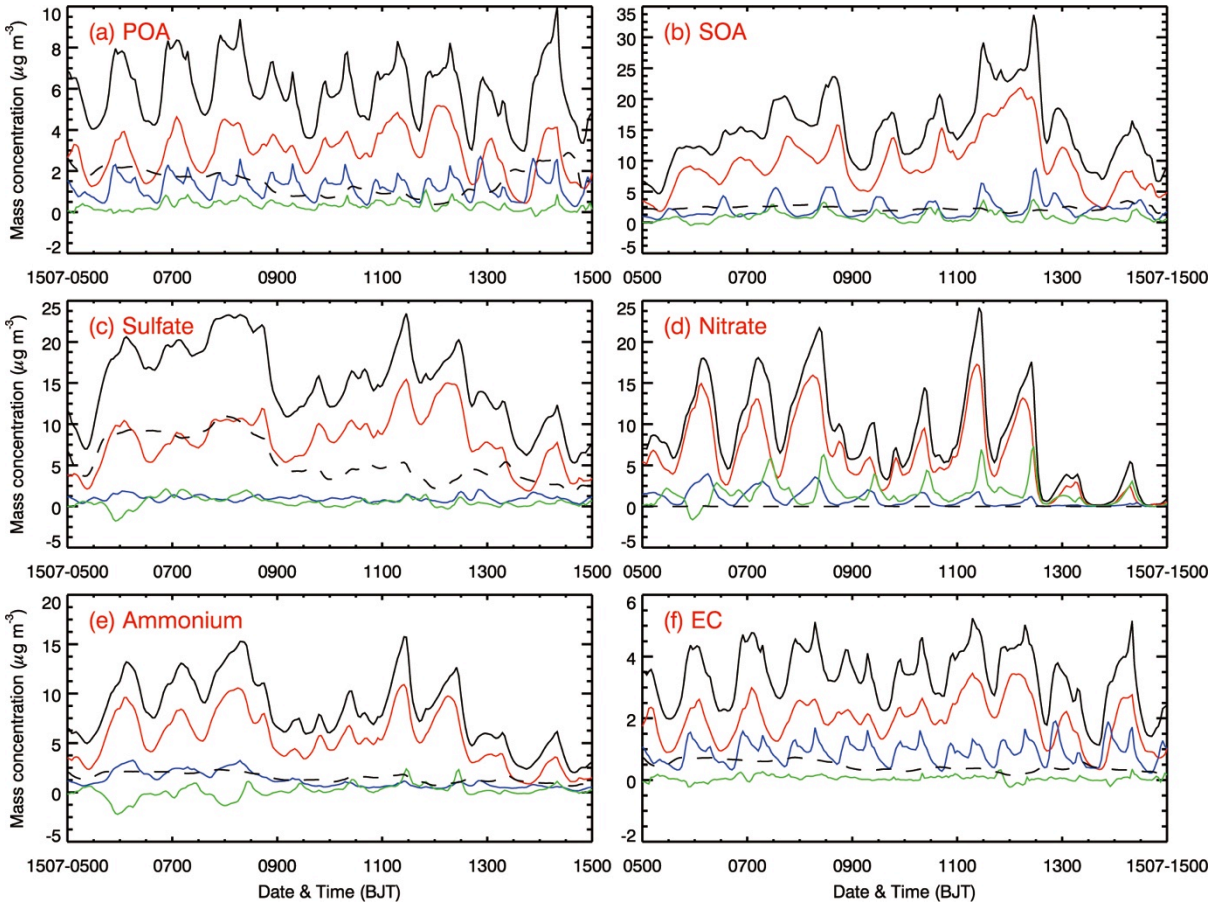
(a) POA
(b) SOA
(c) Sulfate
(d) Nitrate
(e) Ammonium
(f) EC
Mass concentration (μg m-3)
1507-0500
0700
0900
1100
1300
1500
0500
1507-1500
Date & Time (BJT)

Figure 11